



Integrated modeling of canopy photosynthesis, fluorescence, and the transfer of energy, mass, and momentum in the soil–plant–atmosphere continuum (STEMMUS–SCOPE v1.0.0)

Yunfei Wang^{1,2,3,5}, Yijian Zeng³, Lianyu Yu³, Peiqi Yang³, Christiaan Van der Tol³, Qiang Yu⁵, Xiaoliang Lü⁵, Huanjie Cai^{1,2}, and Zhongbo Su^{3,4}

¹College of Water Resources and Architectural Engineering, Northwest Agriculture and Forestry University, Yangling, China

²Institute of Water Saving Agriculture in Arid Regions of China (IWSA), Northwest Agriculture and Forestry University, Yangling, China

³Faculty of Geo-Information Science and Earth Observation, University of Twente, Enschede, the Netherlands

⁴Key Laboratory of Subsurface Hydrology and Ecological Effects in Arid Region, Ministry of Education, School of Water and Environment, Chang'an University, Xi'an, China

⁵State Key Laboratory of Soil Erosion and Dryland Farming on the Loess Plateau, Institute of Water and Soil Conservation, Northwest Agriculture and Forestry University, Yangling, China

Correspondence: Huanjie Cai (huanjiec@yahoo.com) and Zhongbo Su (z.su@utwente.nl)

Received: 31 March 2020 – Discussion started: 2 June 2020

Revised: 17 January 2021 – Accepted: 20 January 2021 – Published: 11 March 2021

Abstract. Root water uptake by plants is a vital process that influences terrestrial energy, water, and carbon exchanges. At the soil, vegetation, and atmosphere interfaces, root water uptake and solar radiation predominantly regulate the dynamics and health of vegetation growth, which can be remotely monitored by satellites, using the soil–plant relationship proxy – solar-induced chlorophyll fluorescence. However, most current canopy photosynthesis and fluorescence models do not account for root water uptake, which compromises their applications under water-stressed conditions. To address this limitation, this study integrated photosynthesis, fluorescence emission, and transfer of energy, mass, and momentum in the soil–plant–atmosphere continuum system, via a simplified 1D root growth model and a resistance scheme linking soil, roots, leaves, and the atmosphere. The coupled model was evaluated with field measurements of maize and grass canopies. The results indicated that the simulation of land surface fluxes was significantly improved by the coupled model, especially when the canopy experienced moderate water stress. This finding highlights the importance of enhanced soil heat and moisture transfer, as well as dynamic root growth, on simulating ecosystem functioning.

1 Introduction

Root water uptake (RWU) by plants is a critical process controlling water and energy exchanges between the land surface and the atmosphere and, as a result, plant growth. The representation of RWU is an essential component of eco-hydrological models that simulate terrestrial water, energy, and carbon fluxes (Seneviratne et al., 2010; Wang and Smith, 2004). However, most of these models consider the above-ground processes in much greater detail than belowground processes; therefore, they have a limited ability to represent the dynamic response of plant water uptake to water stress. A particular mechanism of importance for plants to mitigate water stress is the compensatory root water uptake (CRWU) which refers to the process by which water uptake from sparsely rooted but well-watered parts of the root zone compensates for stress in other parts (Jarvis, 2011). The failure to account for compensatory water uptake and the associated hydraulic lift from deep subsoil (Caldwell et al., 1998; Espeleta et al., 2004; Amenu and Kumar, 2007; Fu et al., 2016) can lead to significant uncertainties in simulating the

plant growth and corresponding ecohydrological processes (Seneviratne et al., 2010).

Because the spatial (i.e., 1D vertical) pattern of RWU is determined by the spatial distribution of the root system, knowledge of the latter is essential for predicting the spatial distribution of water contents and water fluxes in soils. The distribution of roots and their growth are, in turn, sensitive to various physical, chemical, and biological factors, as well as to soil hydraulic properties that influence the availability of water for plants (Beaudoin et al., 2009). Many attempts have been made in the past to develop root growth models that account for the influence of various environmental factors such as temperature, aeration, soil water availability, and soil compaction. Existing root growth models range from complex, 3D root architecture models (Bingham and Wu, 2011; Leitner et al., 2010; Wu et al., 2005) to much simpler root growth models that are implemented within more complex models such as EPIC (Williams et al., 1989) and DSSAT (Robertson et al., 1993). Most of these models reproduce the measured rooting depth very well, but the distribution of new growth root is based on empirical functions rather than biophysical processes (Camargo and Kemanian, 2016; Table 1).

Modeling RWU requires the representation of above- and belowground processes, which can be realized considering the flow of water from soil through the plant to the atmosphere (i.e., the soil–plant–atmosphere continuum, SPAC model; Guo, 1992). The SPAC model represents a good compromise between simplicity (i.e., a small number of tuning parameters) and the ability to capture non-linear responses of RWU (and subsequently the ecosystem functioning) to drought events. Specifically, the SPAC model calculates the CRWU term using the gradient between the leaf water potential and the soil water potential of each soil layer. The most important parameters in the SPAC model include the leaf water potential, stomatal resistance, and the root resistance. Different from other macroscopic models using the root distribution function, the SPAC model explicitly needs the root length density at each soil layer to calculate the root resistance for each soil layer (Deng et al., 2017). The most practical method for obtaining the root length density is using a root growth model.

On other hand, remote sensing of solar-induced chlorophyll fluorescence (SIF) has been deployed to understand and monitor the ecosystem functioning under drought stress using models for vegetation photosynthesis and fluorescence (Zhang et al., 2018, 2020; Mohammed et al., 2019; Shan et al., 2019). SCOPE (Soil Canopy Observation, Photochemistry, and Energy Fluxes) is one such model and simulates canopy reflectance and fluorescence spectra in the observation directions as well as photosynthesis and evapotranspiration as functions of leaf optical properties, canopy structure, and weather variables (Van der Tol et al., 2009). The SCOPE model provides a valuable means to study the link between remote sensing signals and ecosystem functioning; however, it does not consider the water budget in soil and vegetation.

As such, there is no explicit parametrization of the effects of soil moisture variations on the photosynthetic or stomatal parameters. Consequently, soil moisture effects are only “visible” in SCOPE if the lack of soil moisture affects the optical or thermal remote sensing signals (i.e., during water stress periods). The lack of such a link between soil moisture availability and remote sensing signals compromises the capacity of SCOPE to simulate and predict drought events on vegetation functioning.

The change in vegetation optical appearance as a result of soil moisture variations can only partially explain the soil moisture effect on ecosystem functioning (Bayat et al., 2018), which leads to considerably biased estimations of the gross primary productivity (GPP) and evapotranspiration (ET) under water-limited conditions. This presents a challenge with respect to using SCOPE for ecosystems in arid and semiarid areas, where water availability is the primary limiting factor for vegetation functioning. This challenge becomes even more relevant considering that soil moisture deficit or “ecological drought” is expected to increase in both frequency and severity in nearly all ecosystems around the world (Zhou et al., 2013). Bayat et al. (2019) incorporated the SPAC model into SCOPE to address water-stressed conditions at a grassland site, but the coupled model neglected the dynamic root distribution in different soil layers, and soil moisture only serves as a model input when it comes from measurements.

In this study, the modeling of aboveground photosynthesis, fluorescence emission, and energy fluxes in the vegetation layer by SCOPE will be fully coupled with a two-phase mass and heat transfer model – the STEMMUS model (Simultaneous Transfer of Energy, Mass and Momentum in Unsaturated Soil; a more detailed description of STEMMUS can be found in Sect. 2), by considering RWU based on a root growth model. The root growth model and the corresponding resistance scheme (from soil, through roots and leaves, to atmosphere) will be integrated for the dynamic modeling of water stress and the root system, enabling the seamless modeling of soil–water–plant energy, water, and carbon exchanges as well as SIF, thereby directly linking the vegetation dynamics (and its optical and thermal appearance) at the process level to soil moisture variability.

The rest of this article is structured as follows: Sect. 2 describes the coupling scheme between SCOPE and STEMMUS and the data that were used to validate the coupled model; Sect. 3 verifies the coupled STEMMUS–SCOPE model using a maize agroecosystem and a grassland ecosystem located in semiarid regions and explores the dynamic responses of the leaf water potential and root length density to water stress; and the summary of this study and the further challenges are addressed in Sect. 4.

Table 1. Comparison of land surface models (LSMs) and crop models in terms of sink term calculation of soil water balance. CRWU stands for compensatory root water uptake.

Model	Sink term calculation of soil water balance	Root water uptake process			
		Hydraulic redistribution (Richards and Caldwell, 1987)	Compensatory uptake (Jarvis, 2011)	Root distribution	
LSMs	CLM5.0	Root length density of each soil layer; water stress is applied by the hydraulic conductance model (Lawrence et al., 2020)	Extreme case of CRWU	Following Darcy's law for porous media flow equations	Empirical function depends on the plant functional type
	CLM4.5	Actual transpiration, root fraction of each soil layer, and soil integral soil water availability (Fu et al., 2016)	The Ryel et al. (2002) function	Not considered	Empirical function
	CLM4.0	Actual transpiration, root fraction of each soil layer, and integral soil water availability (Couvreur et al., 2012, Sulis et al., 2019)	HRWU scheme (RWU model based on hydraulic architecture)	HRWU scheme	Empirical function
	CLM3 & IBIS2	Actual transpiration, physical root distribution, and the water availability in each layer (Zheng and Wang, 2007)	The Ryel et al. (2002) function	Dynamic root water uptake	Empirical function
	CoLM	Potential transpiration, root fraction in each layer, and water stress factor (Zhu et al., 2017)	The Ryel et al. (2002) and the Amenu and Kumar (2007) function	Empirical approach with a compensatory factor	Empirical function
	JULES	Potential transpiration, root fraction of each soil layer, and a weighted water stress in each layer (Eller et al., 2020)	Not considered	Not considered	Exponential distribution with depth
	Noah-MP	Based on the gradient in water potentials between root and soil, and root surface area (Niu et al., 2020)	Extreme case of CRWU	Following Darcy's law for porous media flow equations	Process-based 1D root surface area growth model

Table 1. Continued.

Model	Sink term calculation of soil water balance	Root water uptake process			
		Hydraulic redistribution (Richards and Caldwell, 1987)	Compensatory uptake (Jarvis, 2011)	Root distribution	
CABLE	Based on the gradient in water potentials between the leaf, stem, and the weighted average of the soil (De Kauwe et al., 2020)	Extreme case of CRWU	Following Darcy's law for porous media flow equations	Empirical function	
Crop models	APSIM	Potential transpiration and water supply factor but neglects root distribution (Keating et al., 2003)	Not considered	Not considered	Empirical function
CropSyst	Difference in water potential between the soil and the leaf, and a total soil–root–shoot conductance (Stöckle et al., 2003)	Not considered	Considered by the leaf and soil water potential	Linear decrease in soils with no limitations on root exploration	
DSSAT	Water uptake per unit of root length is computed as an exponential function, and the actual RWU is the minimum of potential transpiration and the maximum capacity of root water uptake (Jones et al., 2003)	Not considered	Water uptake per unit of root length as a function of soil moisture	Using an empirical function	
EPIC	EPIC assumes that water is used preferentially from the top layers, and the potential water supply rate decreases exponentially downward (Williams et al., 2014)	Not considered	Not considered	Not considered	
SWAP	Based on the potential transpiration, root fraction, and an empiric stress factor relationship (van Dam, 2000)	Not considered	Based on soil water potential	Function of relative rooting depth	
WOFOST	The simplest one, it calculates water uptake as a function of the rooting depth and the water available at that rooting depth without regard for the soil water distribution with depth (Supit et al., 1994)	Not considered	Not considered	Empirical function	

Table 1. Continued.

Model	Sink term calculation of soil water balance	Root water uptake process		
		Hydraulic redistribution (Richards and Caldwell, 1987)	Compensatory uptake (Jarvis, 2011)	Root distribution
SPACSYS	According to empirical root length density distribution in a soil layer, potential transpiration, and soil moisture (Wu et al., 2005)	Not considered	Not considered	1D (empirical function) or 3D root system (process based)
STICS	Based on the potential transpiration, root fraction, and soil water distribution, but not process based (Beaudoin et al., 2009)	Not considered	Not considered	1D root length density profile

2 Methodology and data

2.1 SCOPE and SCOPE_SM models

SCOPE is a radiative transfer and energy balance model (Van der Tol et al., 2009). It simulates the transfer of optical, thermal, and fluorescent radiation in the vegetation canopy and computes ET using an energy balance routine. SCOPE includes a radiative transfer module for incident solar and sky radiation to calculate the top-of-canopy outgoing radiation spectrum, net radiation, and absorbed photosynthetically active radiation (aPAR); a radiative transfer module for thermal radiation emitted by soil and vegetation to calculate the top-of-canopy outgoing thermal radiation and net radiation; an energy balance module for latent heat, sensible heat, and soil heat flux; and a radiative module for chlorophyll fluorescence to calculate the top-of-canopy SIF (the observation zenith angle was set as 0° in this study).

Compared with other radiative transfer models that simplify the radiative transfer processes based on Beer's law, SCOPE has well-developed radiative transfer modules that consider the various leaf orientation and multiple scattering. SCOPE can provide detailed information about the net radiation of every leaf within the canopy. Furthermore, SCOPE incorporates an energy balance model that predicts not only the temperature of leaf but also the soil surface temperature (i.e., a vital boundary condition needed by STEMMUS). In the original SCOPE model, soil is treated in a very simple way with several empirical functions describing the ground heat storage. Later, Bayat et al. (2019) extended the SCOPE model by including the moisture effects on the vegetation canopy, which resulted in the SCOPE_SM model. This model takes soil moisture as input and predicts the effects on several processes of the vegetation canopy using the SPAC

concept. Appendix A1 lists the main equations for calculating the water stress factor within SCOPE (Bayat et al., 2019), and the reader is referred to Van der Tol et al. (2009) for a detailed formulation of SCOPE.

SCOPE_SM provides the basic framework to couple SCOPE with a soil process model. However, both SCOPE and SCOPE_SM ignored the soil heat and mass transfer processes and the dynamics of root growth. This can be overcome by introducing the STEMMUS model.

2.2 STEMMUS model

The STEMMUS model is a two-phase mass and heat transfer model with explicit consideration of the coupled liquid, vapor, dry air, and heat transfer in unsaturated soil (Zeng et al., 2011a, b; Zeng and Su, 2013; Yu et al., 2016, 2018). STEMMUS provides a comprehensive description of water and heat transfer in the unsaturated soil, which can compensate for what is currently neglected in SCOPE. In STEMMUS, the soil layers can be set in a flexible manner, which is an improvement on the previous SPAC model that only considered the whole root zone soil water content as fixed layers (Williams et al., 1996). The water and heat transfer processes are vital for vegetation phenology development as well as freeze–thaw processes. The boundary condition needed by STEMMUS includes surface soil temperature, which is the output of SCOPE. In addition, STEMMUS already contains an empirical equation to calculate root water uptake and a simplified root growth module to calculate root fraction profile. As such, STEMMUS has an ideal model structure to be coupled with SCOPE. The main governing equations of STEMMUS are listed in Appendix A2.

2.3 Dynamic root growth and root water uptake

To obtain the root resistance of each soil layer, we incorporated a root growth module to simulate the root length density profile (see Appendix A3). The simulation of root growth refers to the root growth module in the INRA STICS crop growth model (Beaudoin et al., 2009), which includes the calculations of root front growth and root length growth. The root front growth is a function of temperature, with the depth of the root front beginning at the sowing depth for sown crops and at an initial value for transplanted crops or perennial crops (Beaudoin et al., 2009). The root length growth is calculated in each soil layer, considering the net assimilation rate and the allocation fraction of net assimilation to root, which is, in turn, a function of leaf area index (LAI) and root zone water content (Krinner et al., 2005). The root length density profile is then used to calculate the root resistance to water flow radially across the roots, soil hydraulic resistance, and plant axial resistance to flow from the soil to the leaves (see Appendix A4).

2.4 STEMMUS–SCOPE v1.0.0 coupling

The coupling starts with an initial soil moisture (SM) profile simulated by STEMMUS, which enables the calculation of the water stress factor as a reduction factor of the maximum carboxylation rate (V_{cmax}). SCOPE v1.73 is then used to calculate net photosynthesis (A_n) or gross primary productivity (GPP), soil respiration (R_s), energy fluxes (net radiation, R_n ; latent heat, LE ; sensible heat, H ; and soil heat flux, G), transpiration (T), and SIF, which is passed to STEMMUS as the root water uptake (RWU). Then, the gross primary production (GPP) can be calculated based on A_n . Surface soil moisture is also used in calculating soil surface resistance and then calculating soil evaporation (E). Furthermore, SCOPE can calculate soil surface temperature (T_{s0}) based on energy balance, which is subsequently used as the top boundary condition of STEMMUS, and leaf water potential (LWP), which is a parameter to reflect plant water status, can be calculated through iteration. Based on RWU, STEMMUS calculates the soil moisture in each layer at the end of the time step, and the new soil moisture profile will be the soil moisture at the beginning of next time step, which is repeated as such until the end of simulation period. The time step of STEMMUS–SCOPE is flexible, and the time step used in this study was 30 min. Figure 1 shows the coupling scheme of STEMMUS and SCOPE, and Table B1 in the Appendix shows all of the parameter values used in this study.

2.5 Evapotranspiration partitioning

Most studies in partitioning evapotranspiration (ET) use sap flow and microlysimeter data from in situ measurements. In this study, we used a simple and practical method to separate evaporation (E) and transpiration (T) proposed by Zhou

et al. (2016). Although the behavior of plant stomata is influenced by environmental factors, the potential water use efficiency ($uWUE_p$, $g\ C\ hPa^{0.5}\ (kg\ H_2O)^{-1}$) at the stomatal scale in the ecosystem with a homogeneous underlying surface is assumed to be nearly constant, and variations in actual $uWUE$ ($g\ C\ hPa^{0.5}\ (kg\ H_2O)^{-1}$) can be attributed to the soil evaporation (Zhou et al., 2016). Thus, the method can be used to estimate T and E with the quantities of ET, $uWUE$, and $uWUE_p$. Another assumption of this method is that the ecosystem T is equal to ET at some growth stages, so $uWUE_p$ can be estimated using the upper bound of the ratio of $GPP\sqrt{VPD}$ to ET (here VPD refers to the vapor pressure deficit; Zhou et al., 2014, 2016).

Zhou et al. (2016) used the 95th quantile regression between $GPP\sqrt{VPD}$ and ET to estimate $uWUE_p$, and they showed that the 95th quantile regression for $uWUE_p$ at flux tower sites was consistent with the $uWUE$ derived at the leaf scale for different ecosystems. In addition, the variability in seasonal and interannual $uWUE_p$ was relatively small for a homogeneous canopy. Therefore, the calculations of $uWUE_p$, $uWUE$, and T at the ecosystem scale were as follows:

$$uWUE_p = \frac{GPP\sqrt{VPD}}{T} \quad (1)$$

$$uWUE = \frac{GPP\sqrt{VPD}}{ET} \quad (2)$$

$$\frac{T}{ET} = \frac{uWUE}{uWUE_p} \quad (3)$$

The calculation of the VPD was based on air temperature and relative humidity data, and the method of gap-filling was the marginal distribution sampling (MDS) method proposed by Reichstein et al. (2005). To calculate GPP, the complete series of net ecosystem exchange (NEE) was partitioned into gross primary production (GPP) and respiration (R_e) using the method proposed by Reichstein et al. (2005). Finally, ET was calculated using the latent heat flux and air temperature. Based on GPP, ET, and VPD data, T can be calculated using the method proposed by Zhou et al. (2016).

2.6 Study site and data description

To evaluate the performance of STEMMUS–SCOPE in modeling ecohydrological processes, simulation was conducted to compare STEMMUS–SCOPE with SCOPE, SCOPE_SM, and STEMMUS using observations over a C_4 cropland (summer maize: from 11 June to 10 October 2017) at the Yangling station ($34^{\circ}17' N$, $108^{\circ}04' E$; 521 m a.s.l.) and a C_3 grassland at the Vaira Ranch (US-Var) FLUXNET site ($38^{\circ}25' N$, $120^{\circ}57' W$; 129 m a.s.l.; annual grasses: from 1 June to 8 August 2004). The seasonal variation in precipitation, irrigation, and SM for these two sites are presented in Fig. 2, and the differences in soil surface resistance, water stress factor (WSF), ET, photosynthesis, soil surface temperature (T_{s0}), root water

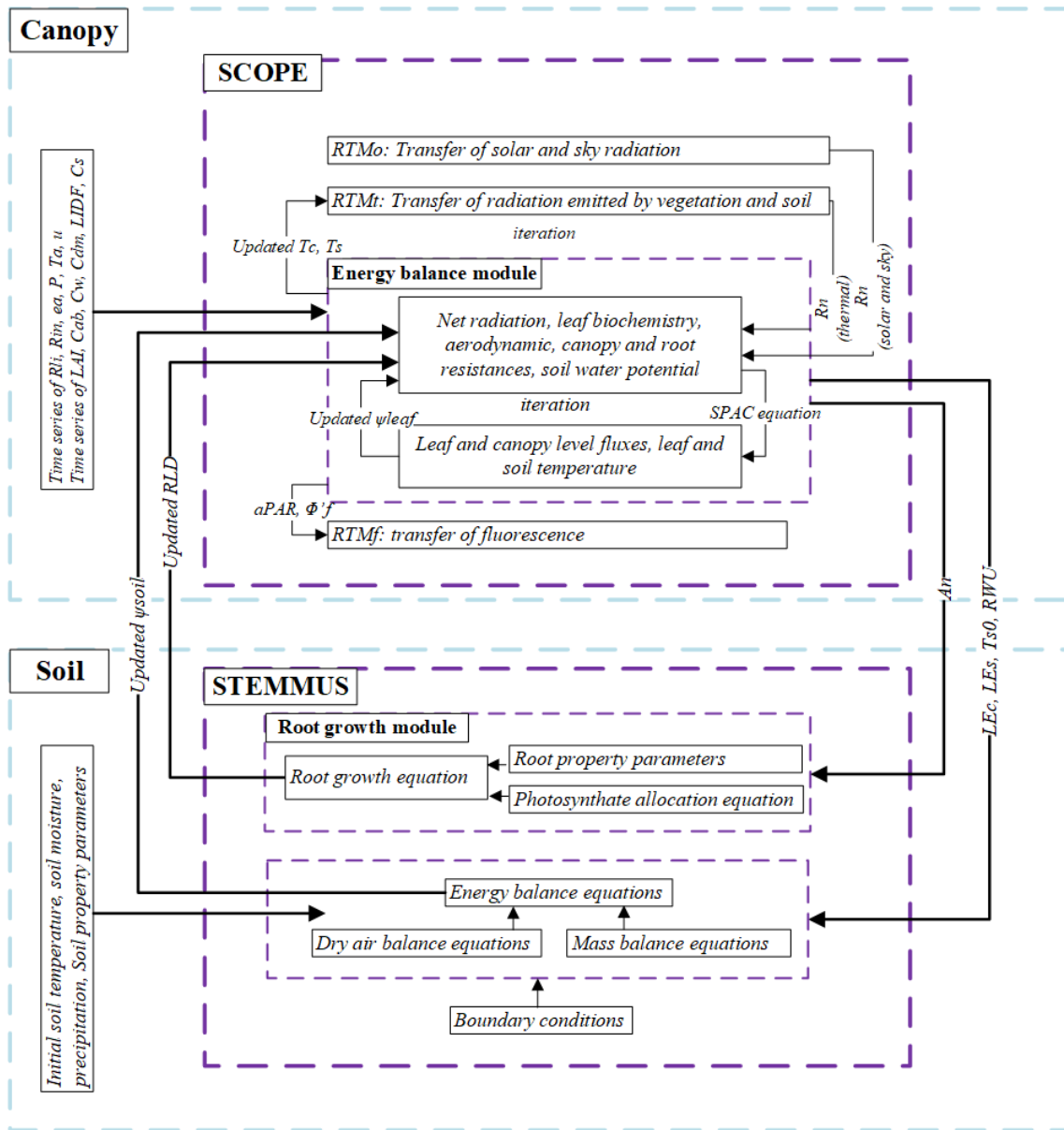


Figure 1. The coupling scheme of STEMMUS–SCOPE. Explanations for the symbols are given in Table B1 in the Appendix.

uptake (RWU), and leaf water potential (LWP) between these four models are presented in Table 2. In this study, the LAI data of the Vaira Ranch (US-Var) FLUXNET site were from the MODIS 8 d LAI product instead of the field-measured LAI used by Bayat et al. (2019). For the soil water content employed by SCOPE_SM, the averaged root zone soil moisture was used for Yangling station, and the soil moisture at 10 cm depth was used for the Vaira Ranch site. For more detailed descriptions of these sites and data, the reader is referred to Wang et al. (2019, 2020a) and Bayat et al. (2018, 2019).

2.7 Performance metrics

The metrics used to evaluate the performance of the coupled STEMMUS–SCOPE model include the (1) root-mean-square error (RMSE), (2) coefficient of determination (R^2), and (3) the index of agreement (d). They are calculated as follows:

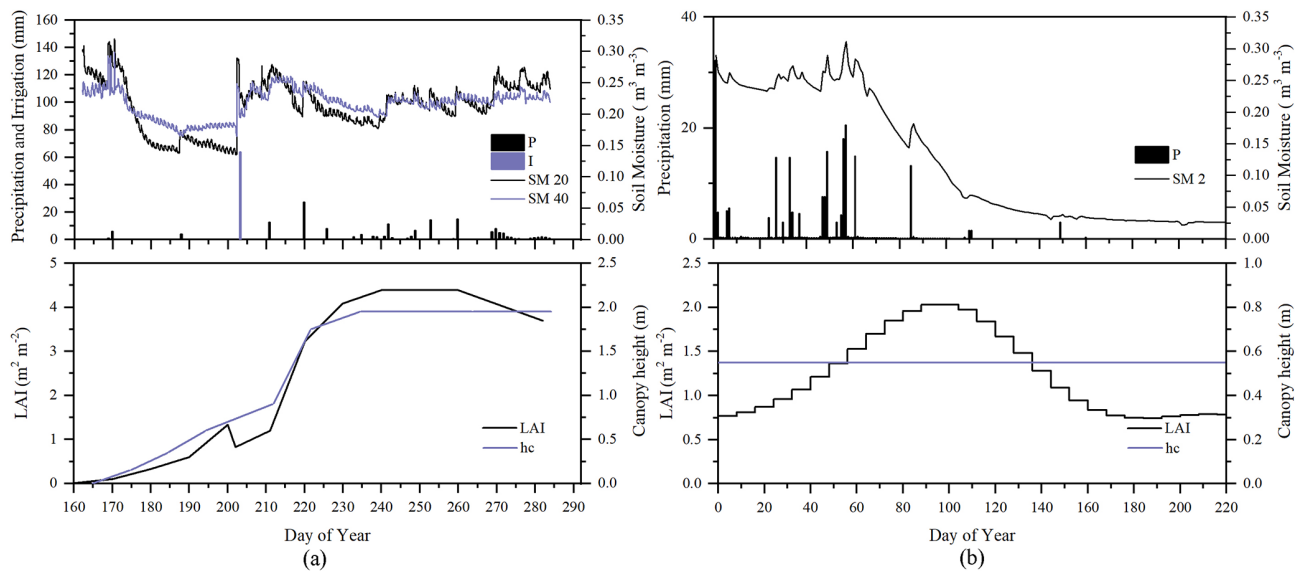


Figure 2. Seasonal variation in precipitation (P); irrigation (I); soil moisture at 2 (SM 2), 20 (SM 20), and 40 cm depth (SM 40); leaf area index (LAI); and canopy height (h_c) for (a) maize cropland at Yangling station and (b) grassland at the Vaira Ranch (US-Var) FLUXNET site.

Table 2. Main differences among SCOPE, SCOPE_SM, STEMMUS, and STEMMUS–SCOPE. The reader is referred to Table B1 in the Appendix for a description of the abbreviations used in this table.

	SCOPE	SCOPE_SM	STEMMUS	STEMMUS–SCOPE
Source	Van der Tol et al. (2009)	Bayat et al. (2019)	Zeng and Su (2013)	This study
Soil surface resistance calculation	Set SM as constant or field-measured surface SM	Field-measured surface SM	Simulated surface SM by itself	Simulated surface SM by itself
WSF calculation	Set SM as constant	Field-measured SM	Simulated SM by itself	Simulated SM by itself
ET calculation	Process based (analogy with Ohm's law)	Process based (analogy with Ohm's law)	Penman–Monteith model or FAO dual crop coefficient method	Process based (analogy with Ohm's law)
Photosynthesis	Farquhar and Collatz model	Farquhar and Collatz model	Absent	Farquhar and Collatz model
Radiation transfer	SAIL4 model	SAIL4 model	Based on Beer's law	SAIL4 model
T_{s0}	Simulated by itself	Simulated by itself	Field measured	Simulated by itself
RWU calculation	Absent	Absent	Based on potential T , root fraction, and soil moisture profile	Based on leaf and soil water potential
LWP calculation	Absent	Calculated by iteration	Absent	Calculated by iteration
Root growth	Absent	Absent	Empirical model	Process-based model

$$\text{RMSE} = \sqrt{\frac{1}{n} \sum_{i=1}^n (P_i - O_i)^2}, \quad (4)$$

$$R^2 = \frac{\left[\sum_{i=1}^n (P_i - \bar{P})(O_i - \bar{O}) \right]^2}{\sum_{i=1}^n (P_i - \bar{P})^2 \sum_{i=1}^n (O_i - \bar{O})^2}, \quad (5)$$

$$d = 1 - \frac{\sum_{i=1}^n (P_i - O_i)^2}{\sum_{i=1}^n (|P_i - \bar{O}| + |O_i - \bar{O}|)^2}, \quad (6)$$

where P_i is the i th predicted value, O_i is the i th observed value, \bar{O} is the average of the observed values, and n is the number of samples.

3 Results and discussion

3.1 Soil moisture modeling

As the soil moisture profile was not available at the US-Var site, the comparisons of simulated soil moisture (SM) at Yangling station using STEMMUS and STEMMUS–SCOPE with observed values are presented in Fig. 3. For the simulation of soil moisture at 20 cm, the RMSE values were 0.023 and 0.021 and the d values were 0.90 and 0.91 for STEMMUS and STEMMUS–SCOPE, respectively. For the simulation of soil moisture at 40 cm, the RMSE values were 0.017 and 0.021 and the d values were 0.83 and 0.74, respectively. The simulated soil moisture at 20 cm depth agreed with the observed values in terms of the seasonal pattern. Although a slight overestimation occurred at initial and late stages, the dynamics in soil moisture resulting from precipitation or irrigation were well captured. Per the nature of the two models, the coupling of SCOPE with STEMMUS is not expected to improve the simulation of soil moisture. However, compared with SCOPE_SM, which used soil moisture measurements as inputs, the coupled STEMMUS–SCOPE model improves the simulation of soil moisture dynamics as measured. The deviation between the model simulations and the measurements can be attributed to the following two potential reasons. First, the field observations contain errors to a certain extent, and the soil moisture sensors may be not well calibrated. Second, in this simulation, we assumed that the soil texture was homogeneous in the vertical profile, whereas, in reality, the soil properties (e.g., soil bulk density and saturated hydraulic conductivity) may vary with depth and at different growth stages due to field management practices. For example, the soil bulk density at 40 cm was much higher than that at 20 cm due to the mechanical tillage, especially in the early stage.

3.2 Soil temperature modeling

Similar to soil moisture, only soil temperatures (T_s) simulated by STEMMUS and STEMMUS–SCOPE at 20 and 40 cm depth at the Yangling site are shown in Fig. 4. In general, both models can capture the dynamics of soil temperature well. For the simulation of temperature at 20 cm, the RMSE values were 2.56 and 2.58 °C and the d values were 0.92 and 0.92 for STEMMUS and STEMMUS–SCOPE, respectively. For the simulation of temperature at 40 cm, the RMSE values were 2.06 and 2.07 °C and the d values were 0.93 and 0.93, respectively. These results indicate that both models can simulate soil temperature well. However, some differences also exist between the simulation and observations. The largest difference occurred on DOY (day of year) 202, when the field was irrigated using the flood irrigation method. This irrigation activity may lead to boundary condition errors (i.e., for soil surface temperature), which cannot be estimated well enough (e.g., there is no monitoring of water temperature from the irrigation). Meanwhile, the measurements may also have some errors during this period. The fact that the observed soil temperature at 20 and 40 cm decreased to almost the same level at the same time indicates a potential pathway for preferential flow in the field (see precipitation and irrigation on DOY 202 in Fig. 2), and the sensors captured this phenomenon. Nevertheless, the model captures the soil temperature dynamics.

3.3 Energy balance modeling

Comparisons of the modeled and observed 30 min net radiation (R_n), sensible heat flux (H), latent heat flux (LE), and soil heat flux (G) using SCOPE, SCOPE_SM, and STEMMUS–SCOPE are presented in Fig. 5 (STEMMUS uses R_n as driving data; therefore, it is not included in the comparison). For net radiation and soil heat flux, the simulations of all three models show good agreement with the observations, and the coefficients of determination (R^2) for SCOPE, SCOPE_SM, and STEMMUS–SCOPE were 0.99, 1.00, and 0.99, respectively. For soil heat flux, the R^2 values for SCOPE, SCOPE_SM, and STEMMUS–SCOPE were 0.81, 0.79, and 0.80, respectively. For latent heat flux, STEMMUS–SCOPE shows better performance than SCOPE and SCOPE_SM, and the R^2 values for SCOPE, SCOPE_SM, and STEMMUS–SCOPE were 0.82, 0.84, and 0.85, respectively. Furthermore, STEMMUS–SCOPE and SCOPE_SM show similar performance in the simulation of sensible heat flux, both of which were better than the performance of SCOPE; the R^2 values for SCOPE, SCOPE_SM, and STEMMUS–SCOPE were 0.70, 0.75, and 0.74, respectively.

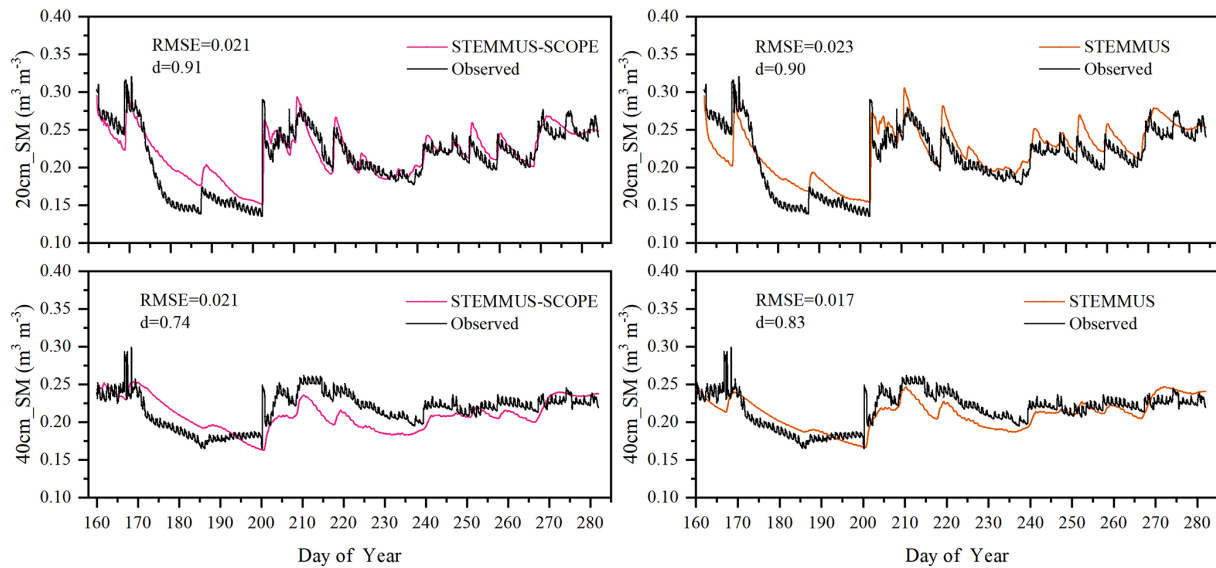


Figure 3. Comparison of modeled and observed soil moisture at 20 (20cm_SM) and 40 cm (40cm_SM) depth for the maize cropland at Yangling station.

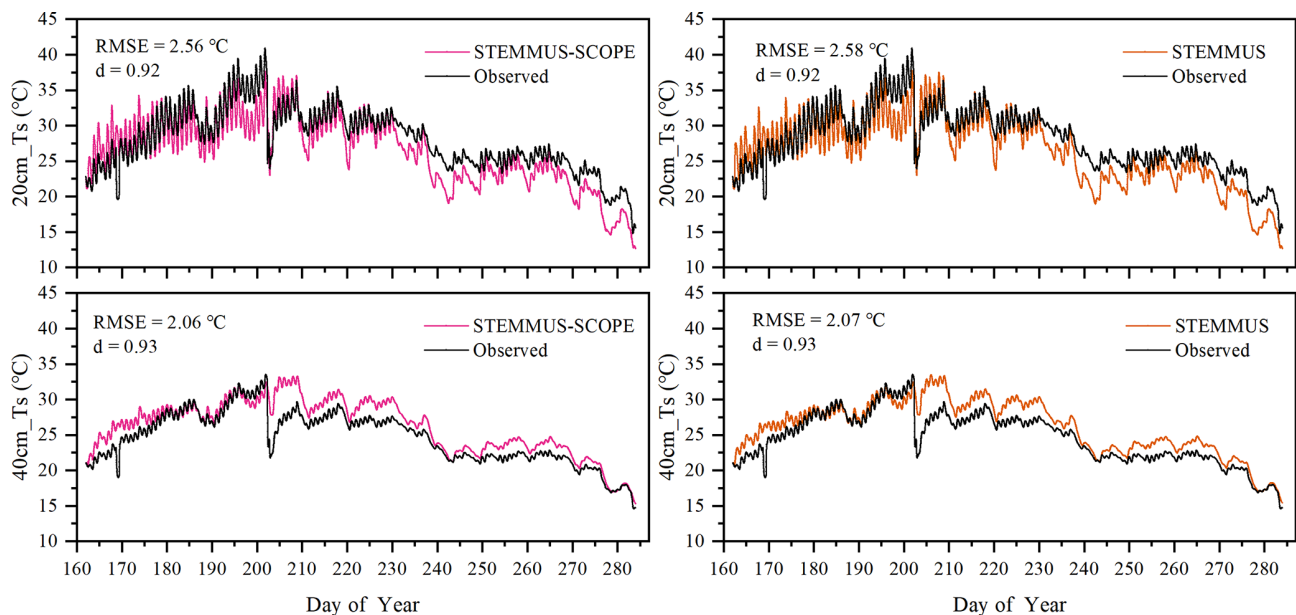


Figure 4. Comparison of observed and modeled soil temperature at 20 (20cm_Ts) and 40 cm (40cm_Ts) depth for the maize cropland at Yangling station.

3.4 Daily ET, T , and E modeling

Simulated daily evapotranspiration (ET) results by SCOPE, SCOPE_SM, STEMMUS, and STEMMUS–SCOPE are presented in Fig. 6. For the Yangling station, the R^2 values for SCOPE, SCOPE_SM, STEMMUS, and STEMMUS–SCOPE were 0.76, 0.82, 0.80, and 0.81, and the RMSEs were 0.84, 0.69, 0.76, and 0.74 mm d^{-1} , respectively. For the US-Var station, the R^2 values for SCOPE, SCOPE_SM, STEMMUS, and STEMMUS–SCOPE were 0.10, 0.66, 0.84,

and 0.89, and the RMSEs were 1.83, 0.63, 0.40, and 0.34 mm d^{-1} , respectively. For the ET simulation by SCOPE, there were large differences between simulations and observations when the vegetation suffered water stress. For SCOPE_SM, STEMMUS, and STEMMUS–SCOPE, the simulated ET values were closer to observations when the vegetation experienced water stress because the dynamics of soil moisture was included in the model. This indicates that STEMMUS–SCOPE, STEMMUS, and SCOPE_SM can

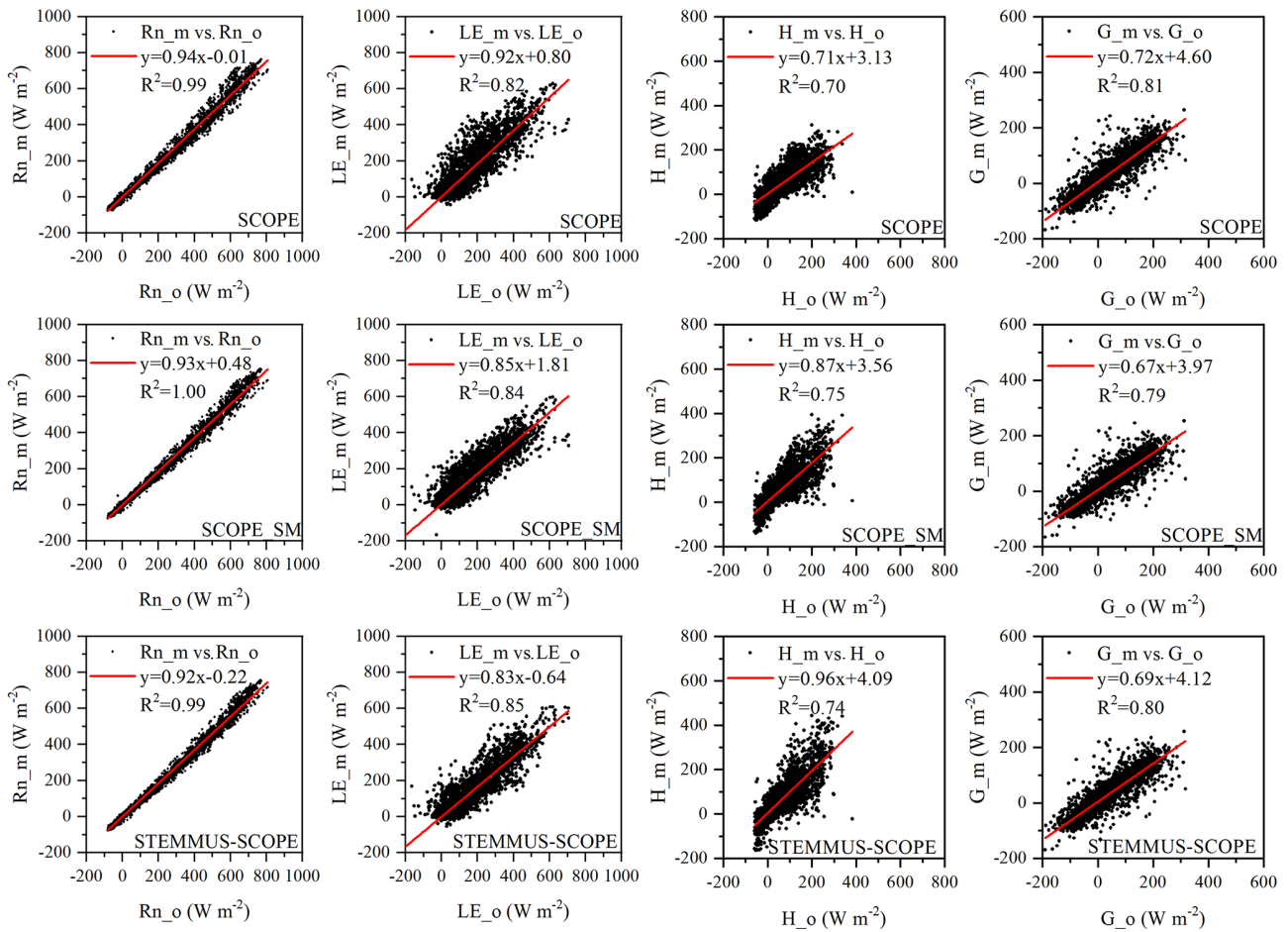


Figure 5. Comparison of modeled and observed 30 min net radiation (R_n), latent heat (LE), sensible heat (H), and soil heat flux (G) by SCOPE, SCOPE_SM, and STEMMUS–SCOPE at Yangling station. The subscripts “_m” and “_o” in each plot indicate modeled and observed quantities, respectively. The regression line is indicated in red, and the corresponding regression equation and R^2 value are given.

predict ET with a relatively higher accuracy, especially when the maize was under water stress (DOY 183–202 at Yangling station and DOY 90–220 at the US-Var site), and STEMMUS–SCOPE and SCOPE_SM performed similarly well. It is noteworthy that although STEMMUS considered the effect of soil moisture on ET, the accuracy of STEMMUS was lower than that of the coupled model (see Fig. 6). The possible reason for this is the better representation of transpiration in the SCOPE model (see Fig. 7), which separates the canopy into 60 layers, whereas STEMMUS only treats the canopy as one layer. Moreover, the coupled model performed better for the grassland than for maize cropland. The reason for this is that the grassland simulation used the dynamic V_{cmax} data, whereas the maize simulation used a constant V_{cmax} data.

The modeled and observed daily transpiration at the maize cropland are presented in Fig. 7, and the modeled transpiration at the grassland site is presented in Fig. 8. For Yangling station, the R^2 values between the simulated and observed transpiration were 0.82, 0.86, 0.79, and 0.86, and the

RMSEs were 0.60, 0.50, 0.67, and 0.50 mm d^{-1} , for SCOPE, SCOPE_SM, STEMMUS, and STEMMUS–SCOPE, respectively. Because it ignored the effect of water stress on transpiration, SCOPE failed to simulate transpiration accurately when the vegetation experienced water stress. As shown in Fig. 6a, SCOPE overestimated transpiration for the maize cropland at Yangling station from DOY 183 to 202 during the water stress period. Compared with SCOPE, SCOPE_SM, STEMMUS, and STEMMUS–SCOPE can capture the reduction in transpiration during the dry period. The performance of STEMMUS–SCOPE and SCOPE_SM was also better than that of STEMMUS. The possible reason for this is the more processed-based consideration of the radiative transfer and energy balance at the leaf level in the coupled STEMMUS–SCOPE model (as in SCOPE_SM) and the more accurate root water uptake (compared with that in SCOPE_SM). Nevertheless, STEMMUS–SCOPE slightly underestimated transpiration when the plant was undergoing severe water stress and slightly overestimated it after the field was irrigated. This is mainly because the actual V_{cmax}

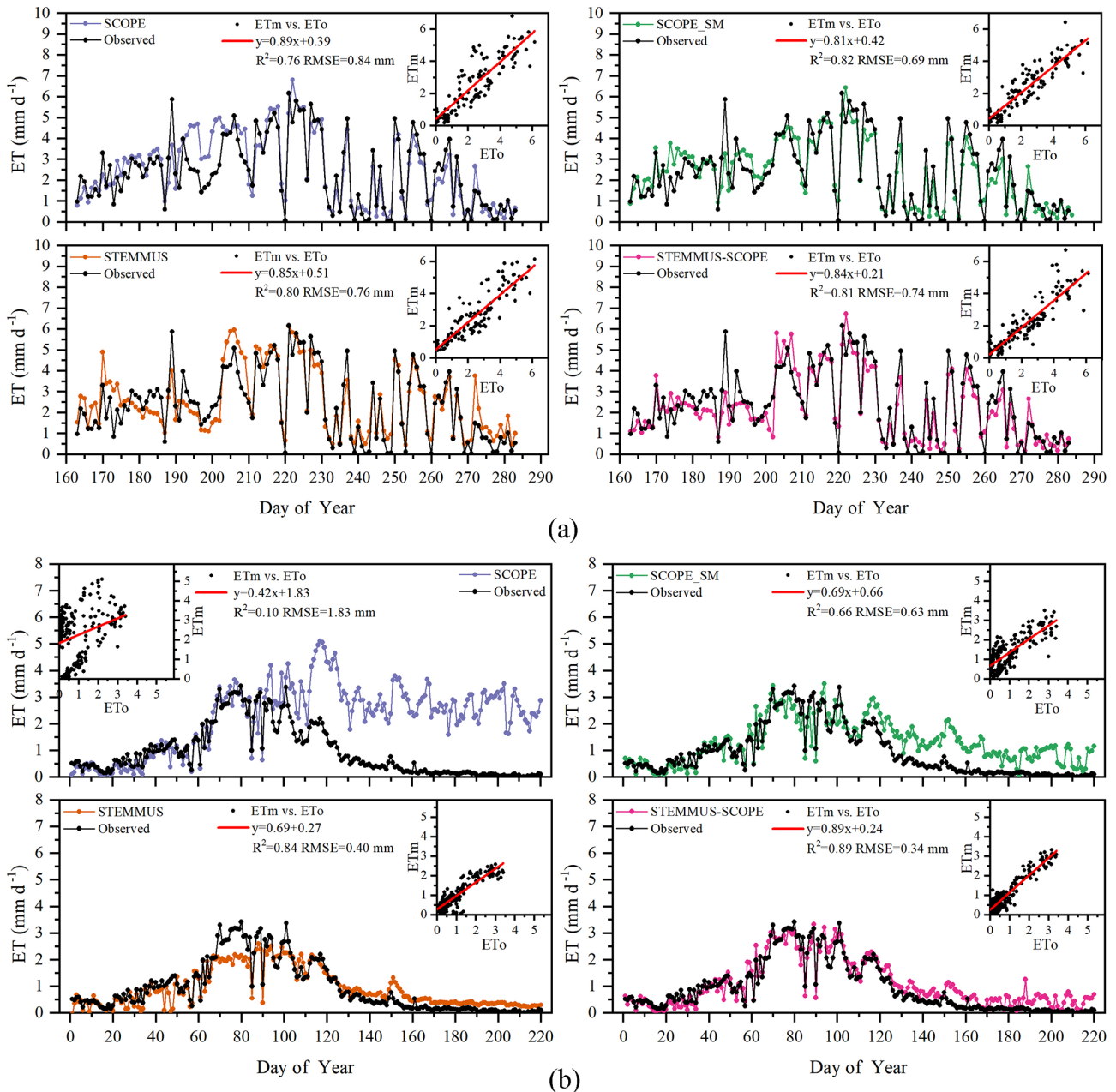


Figure 6. Comparison of modeled and observed daily evapotranspiration (ET) for (a) maize cropland at Yangling station and (b) grassland at the Vaira Ranch (US-Var) FLUXNET site (ETm denotes modeled ET, and ETo denotes observed ET).

was not only influenced by drought but was also related to the leaf nitrogen content (Xu and Baldocchi, 2003), which was not considered in the maize cropland simulation. Although measured T at the grassland was not available, we compared modeled T from the four models (Fig. 7). During the wet season (before DOY 85), the modeled T values from SCOPE, SCOPE_SM, and STEMMUS-SCOPE were similar and were higher than that from STEMMUS from DOY 64 to 82. During the dry season (after DOY 85), due to the simplified consideration of soil processes, the modeled T values

from SCOPE and SCOPE_SM were both much higher than those from STEMMUS and STEMMUS-SCOPE. The reason for the better performance of the coupled model for the grassland (Fig. 6b) is that it also considers the effect of the leaf chlorophyll content (C_{ab}) on V_{cmax} , in addition to a more detailed consideration of water stress as discussed above for the maize cropland.

As shown in Fig. 9 for soil evaporation at Yangling station, the simulated values from STEMMUS-SCOPE are closer to the observations than those from other models. When using

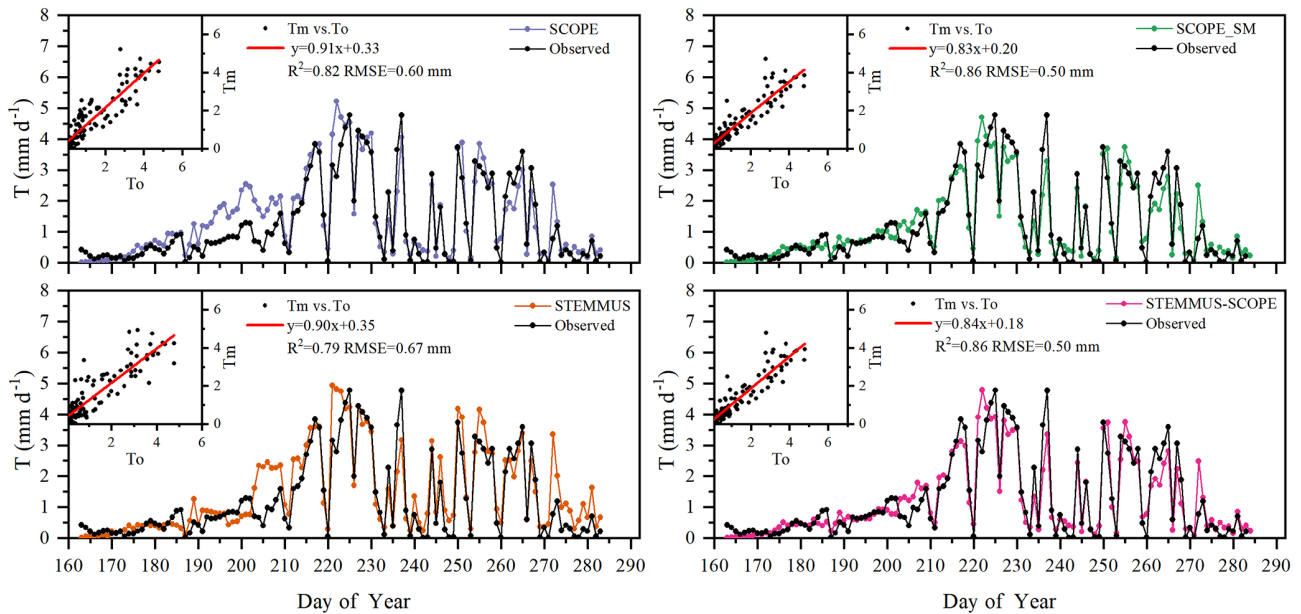


Figure 7. Comparison of modeled and observed daily plant transpiration (T) for the maize cropland at Yangling station (T_m denotes modeled T , and T_o denotes observed T).

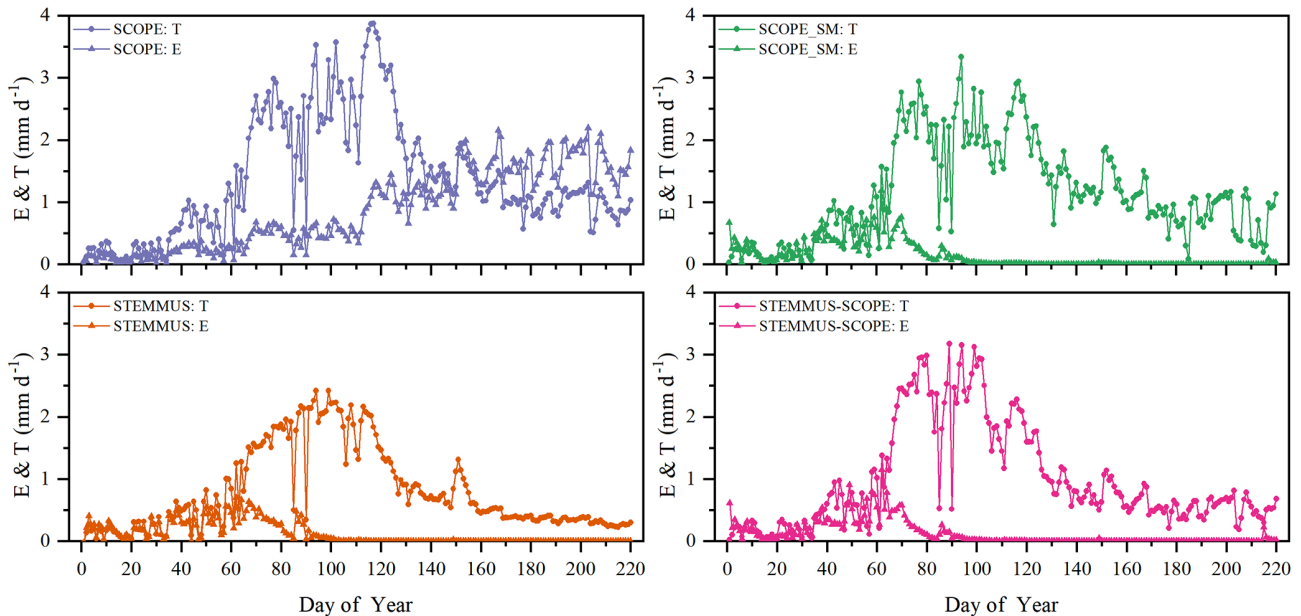


Figure 8. Comparison of modeled daily transpiration (T) and soil evaporation (E) for grassland at the Vaira Ranch (US-Var) FLUXNET site (T denotes transpiration, and E denotes soil evaporation).

SCOPE to simulate soil evaporation, the soil moisture is set as constant (i.e., $0.25 \text{ m}^3 \text{ m}^{-3}$). Therefore, SCOPE generally underestimates soil evaporation when soil moisture is higher than 0.25 and overestimates it when it is lower than 0.25. Here, we use the average soil moisture at the root zone simulated by STEMMUS–SCOPE as the input data for SCOPE and SCOPE_SM in order to calculate soil surface resistance

and soil evaporation. Although STEMMUS can capture variation in soil evaporation reasonably well, it has a higher RMSE than STEMMUS–SCOPE. This is probably attributed to the comprehensive consideration of radiation transfer in SCOPE, which is lacking in STEMMUS. Consequently, the simulation of soil net radiation by the coupled model was more accurate than that from STEMMUS alone. The RMSE

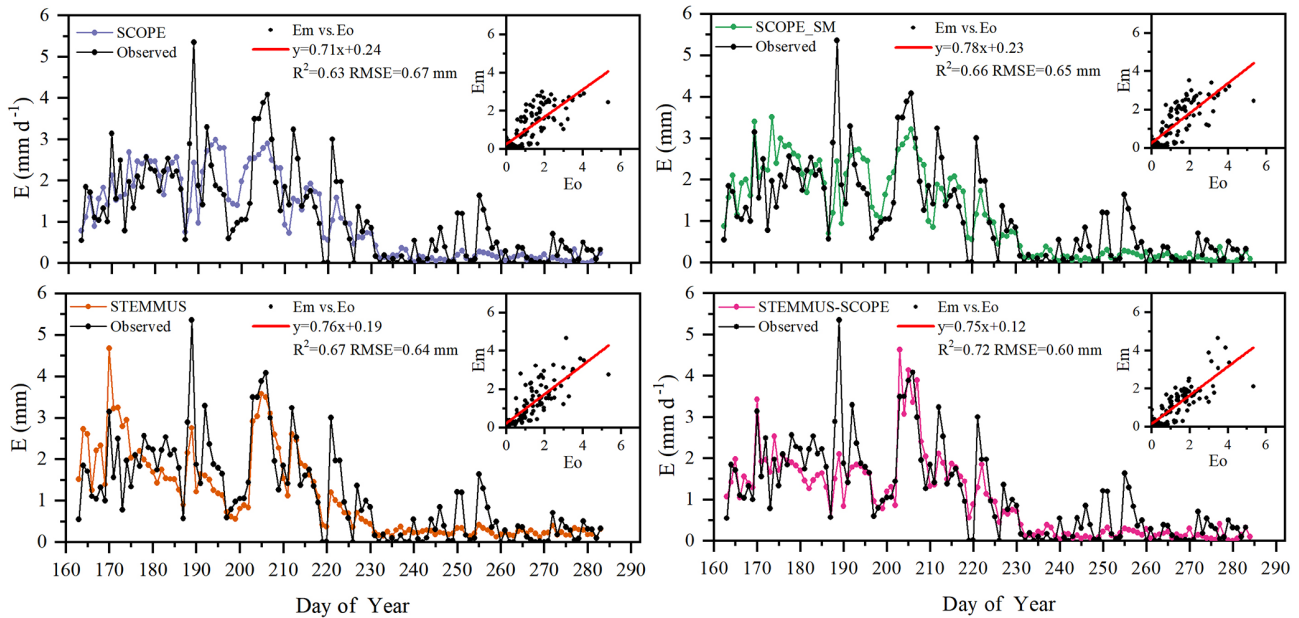


Figure 9. Comparison of modeled and observed daily soil evaporation (E) at Yangling station (E_m denotes modeled E , and E_o denotes observed E).

value for STEMMUS–SCOPE was 0.60 mm d^{-1} , which was lower than those from the other three models (0.67, 0.65, and 0.64 mm d^{-1} , respectively). For STEMMUS–SCOPE, the major differences between simulations and observations occurred on rainy or irrigation days (see Fig. 2a), which may be caused by errors in the estimated soil surface resistance during these periods or the uncertainty of the ET partitioning method. The uncertainty of the ET partitioning method (Zhou et al., 2016) was mainly caused by (1) the uncertainty in the partitioning of GPP (less than 10 %) and R_e based on NEE, which would result in some uncertainty in uWUE; (2) due to the seasonal variation in the atmospheric CO_2 concentration – the assumption of uWUE_p being constant would cause some uncertainty (less than 3 %); (3) the assumption of T being equal to ET sometimes during the growing season would cause some uncertainty when vegetation is sparse. Because the observed E at the US-Var site was not available, a comparison of only modeled E is shown in Fig. 8, in which SCOPE modeled unrealistic E during the dry season, whereas the modeled E values from SCOPE_SM, STEMMUS, and STEMMUS–SCOPE were consistent due to the use of the simulated surface SM as the input for soil evaporation calculation.

3.5 Daily GPP modeling

Simulated GPP from SCOPE, SCOPE_SM, and STEMMUS–SCOPE and observed GPP are presented in Fig. 10. As shown, similar to the simulation of transpiration, SCOPE cannot respond to water stress when simulating GPP. After introducing a soil water stress factor

in STEMMUS–SCOPE and SCOPE_SM, the simulation of GPP was improved in both models. For Yangling station, the consistency between simulated and observed GPP at mid and late stages was higher than that at early and rapid growth stages. The difference usually occurred when soil moisture increased. For the US-Var site, STEMMUS–SCOPE simulated GPP well during the whole period, whereas SCOPE_SM slightly underestimated GPP around DOY 80 when this site transits from the wet season to the dry season. This indicates that only using the surface SM cannot reflect the actual root zone SM when the vegetation is experiencing moderate water stress. Under such conditions, the hydraulic redistribution (HR) and compensatory root water uptake (CRWU) process enable the vegetation to utilize the water in the deep soil layer. Only using the surface soil water content to calculate RWU in SCOPE_SM ignored the effect of the HR and CRWU process, and the effect of water stress was overestimated. However, the surface soil moisture can reflect root zone soil moisture well when the vegetation is not under water stress or severe water stress. A similar underestimation of GPP was also found by Bayat et al. (2019).

3.6 Simulation of leaf water potential (LWP), water stress factor (WSF), and root length density (RLD)

The simulated 30 min leaf water potential and water stress factor at Yangling station are presented in Fig. 11. The leaf water potential was lower when vegetation was suffering water stress compared with other periods. The reason for this is that soil water potential is low due to the low soil moisture, and plants need to maintain an even lower leaf water poten-

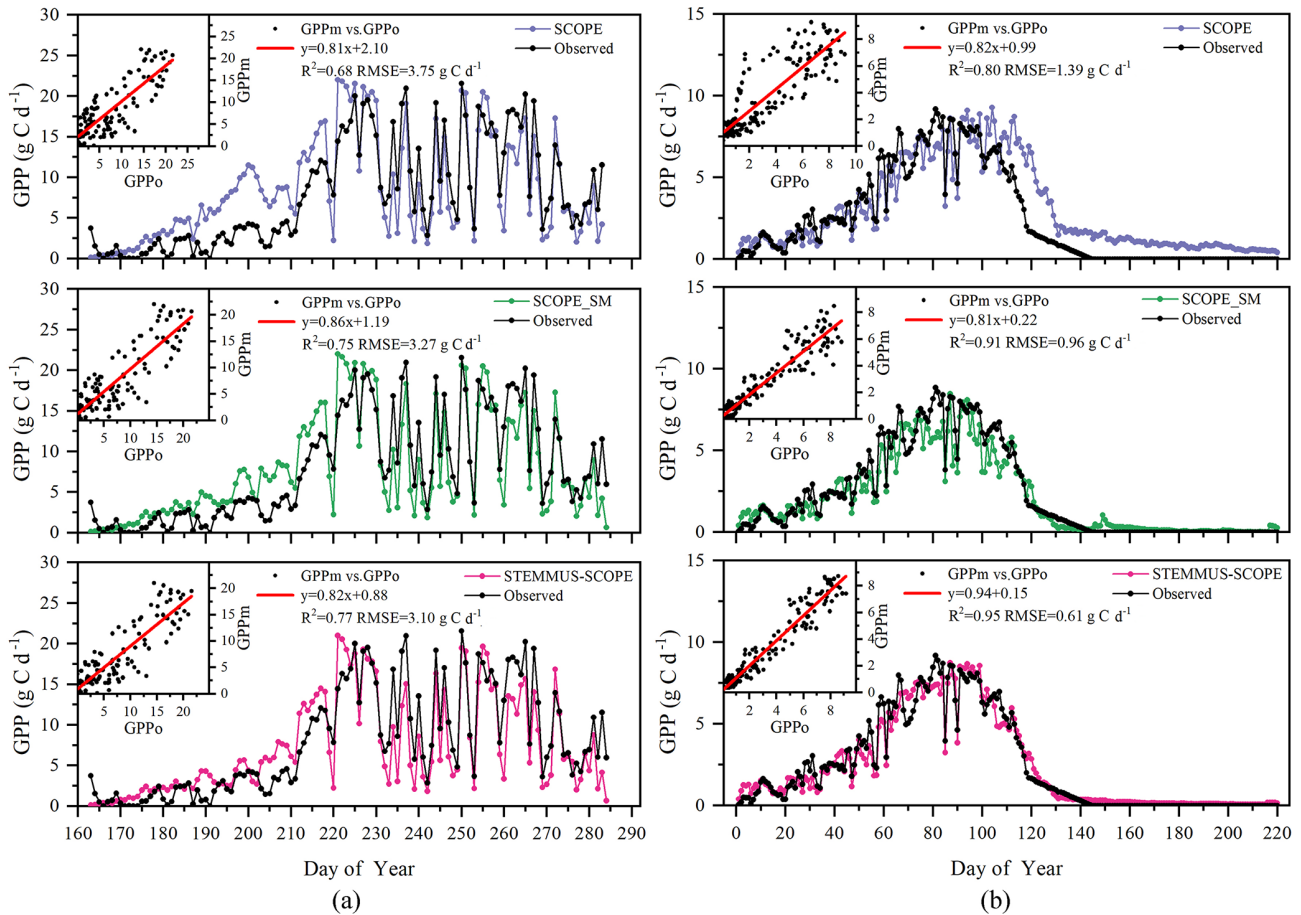


Figure 10. Comparison of modeled and observed daily gross primary production (GPP) for (a) maize cropland at Yangling station and (b) grassland at the Vaira Ranch (US-Var) FLUXNET site (GPPm denotes modeled GPP, and GPPo denotes observed GPP).

tial to suck water from the soil and transfer it to leaves. During mid and late stages, the leaf water potential was sensitive to transpiration demand due to the slowdown of root system growth. As continuous measurements of the leaf water potential are not available, we compared only the magnitude of simulated leaf water potential to measurements reported in the literature.

Many studies have measured midday leaf water potential or dawn leaf water potential. Fan et al. (2015) reported that the leaf water potential of well-watered maize remained high at between -73 and -88 m and that leaf water potential would decrease when the soil water content was lower than 80 % of field capacity. Martineau et al. (2017) reported that the midday leaf water potential of well-watered maize was around -0.82 MPa (about 84.8 m in water pressure head; note that 0.1 MPa is equal to 10.339 m water pressure head) and that the midday leaf water potential decreased to -1.3 MPa (about 134.4 m in water head) when the maize was suffering water stress. Moreover, O’Toole and Cruz (1980) studied the response of leaf water potential to water stress in rice and concluded that the leaf water potential of rice

can be lower than -80 to -120 m when the vegetation was under water stress and the leaves started curling, which was similar to the simulated leaf water potential of maize in this study. Aston and Lawlor (1979) revealed the relationship between transpiration, root water uptake, and leaf water potential of maize. These field studies found that leaf water potential was often very low and reached trough values at midday. Elfving et al. (1972) developed a water flux model based on the SPAC system, evaluated it for orange trees, and reported about -120 m for the trough value of leaf water potential under non-limiting environmental conditions, which was slightly lower than the simulation in this study.

In this study, the calculation of the water stress factor considered the effect of soil moisture and root distribution. The severe water stress occurred from DOY 183 to 202, and the coupled model performed very well during this period. Due to feedback, water stress can also influence root water uptake and root growth and, consequently, influence soil moisture and root dynamics in next time step. This indicates that the water stress equation used in this study can characterize the reduction in V_{Cmax} reasonably well.

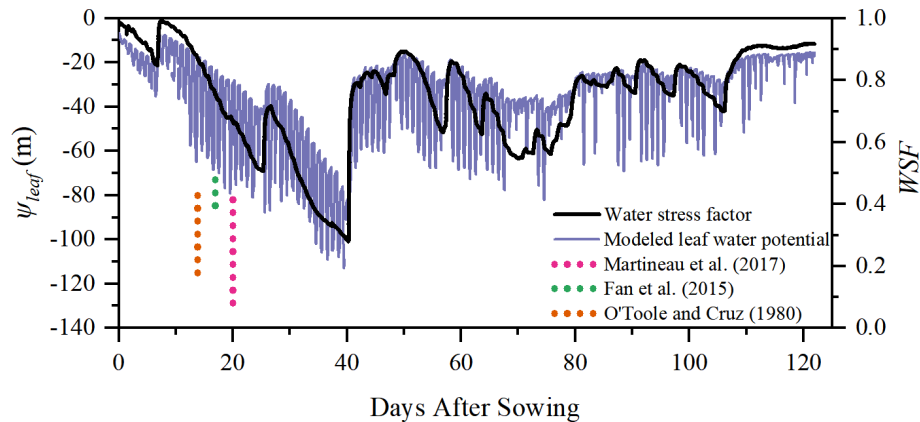


Figure 11. Simulation of ψ_{leaf} (leaf water potential, m) and the WSF (water stress factor) at Yangling station. (The dotted lines represent the range of midday leaf water potential reported at other sites.)

Root length density is another vital parameter in calculating root water uptake. As shown in Table 3, the simulated peak root length density and maximum rooting depth of maize at Yangling station was comparable to the measured values from other sites. Many previous studies have revealed that root length density is influenced by soil moisture, bulk density, tillage, and soil mineral nitrogen (Amato and Ritchie, 2002; Chassot et al., 2001; Schroder et al., 1996). In this study, as we assumed that the soil was homogeneous. STEMMUS–SCOPE considered the effect of soil moisture but neglected the effect of bulk density and soil mineral nitrogen. Amato and Ritchie (2002) also found a similar result to this study with respect to the root length density in a maize field. Peng et al. (2012) studied temporal and spatial dynamics in the root length density of field-grown maize and found that 80 % root length density was distributed at 0–30 cm depth with peak values from 0.86 to 1.00 cm cm^{-3} . Ning et al. (2015) also reported a similar observation of root length density. Chassot et al. (2001) and Qin et al. (2006) reported that root length density can reach 1.59 cm cm^{-3} in the Swiss Midlands. In Stuttgart, Germany, Wiesler and Horst (1994) observed the root growth and nitrate utilization of maize under field conditions. The observed root length density was 2.45–2.80 cm cm^{-3} at 0–30 cm depth, which was much higher than in other studies, and decreased to 0.01 cm cm^{-3} at 120–150 cm depth, which was consistent with the observations of Oikeh et al. (1999) at Samaru, Nigeria. Zhuang et al. (2001b) proposed a scaling model to estimate the distribution of the root length density of field-grown maize. In their study, the measured root length density in Tokyo, Japan, decreased from 0.4 to 0.95 cm cm^{-3} in the top soil layer to about 0.1 cm cm^{-3} in the bottom layer. Zhuang et al. (2001a) observed that the root length density of maize was mainly distributed at 0–60 cm depth, and the maximum values were about 0.9 cm cm^{-3} . These studies indicated that the root length density values were quite variable when this parameter was observed at different sites; never-

theless, the simulated root length density in our study was of an order of magnitude that was similar to the observations from previous studies (Table 3).

3.7 Diurnal variation in T, GPP, SIF, and LWP

Figure 12 shows the modeled and observed 30 min canopy transpiration (T), gross primary production (GPP), solar-induced fluorescence (SIF), and leaf water potential (LWP) from DOY 183 to 202 at Yangling station. The simulations by STEMMUS–SCOPE and SCOPE_SM were consistent with observations, whereas the simulated values from SCOPE were much higher than observations. The performance of STEMMUS–SCOPE and SCOPE_SM was consistent with that of SCOPE in the early morning and late afternoon, when photosynthesis was mainly limited by incident radiation rather than by water stress, intercellular CO_2 concentration, and V_{cmax} . At midday, with increasing incident radiation, photosynthesis was mainly limited by water stress and V_{cmax} , during which time the simulations by STEMMUS–SCOPE and SCOPE_SM were much better than that by SCOPE. The diurnal variation in the observed and modeled GPP was similar to that of T . Due to the lack of observed SIF, only the simulated SIF values were presented. As shown in Fig. 12, the SIF values simulated by STEMMUS–SCOPE and SCOPE_SM were reduced when the vegetation was experiencing water stress, which indicated that both the simulated SIF from STEMMUS–SCOPE and SCOPE_SM can respond to water stress. However, the accuracy of the simulated SIF requires further validation with field observations.

Figure 13 shows the relationship among 30 min GPP, SIF, and LWP on DOY 199 at Yangling station. There was a strong linear relationship between SIF and GPP when the maize was well-watered (Fig. 13a). However, SIF kept increasing, whereas GPP tended to saturate when the maize was suffering water stress. This result is consistent with the previous study conducted for cotton and tobacco leaves (Van

Table 3. Comparison of the peak root length density (RLD; cm cm^{-3}) at Yangling station with that at other sites.

Location	Maximum rooting depth (cm)	Peak RLD (cm cm^{-3})	Soil type	Bulk density (g cm^{-3})	References
Potenza, Italy	100	0.84	Clay loam	1.59–1.69	Amato and Ritchie (2002)
Beijing, China	60	0.78	Silty loam		Peng et al. (2012)
Alize, Stuttgart, Germany	150	2.45	Clay	1.5–1.7	Wiesler and Horst (1994)
Brummi, Stuttgart, Germany	150	2.80	Clay	1.5–1.7	Wiesler and Horst (1994)
Swiss Midlands	100	1.59	Sandy silt	1.21–1.55	Qin et al. (2006)
Samaru, Nigeria	90	2.78	Loamy soil	1.39–1.67	Oikeh et al. (1999)
Tokyo, Japan	58	0.95	Sandy loam	0.61–0.80	Zhuang et al. (2001a, b)
Yangling, China	121	0.74	Sandy loam	1.41	This study

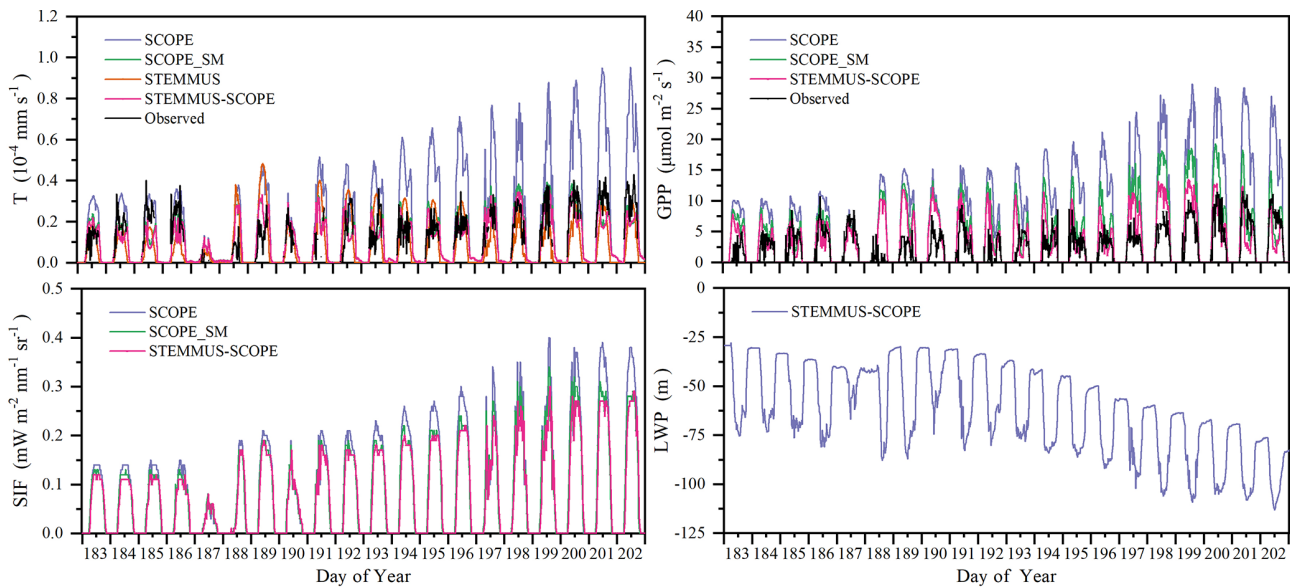


Figure 12. Comparison of modeled and observed 30 min transpiration (T), gross primary production (GPP), top-of-canopy solar-induced fluorescence (SIF), and leaf water potential (LWP) at Yangling station.

der Tol et al., 2014). Because SCOPE_SM used the averaged root zone SM and ignored vertical root and soil water distribution, it overestimated GPP and SIF. When the maize was experiencing drought, the LWP was maintained at a low level. With GPP and T increasing, the plant decreased LWP in order to extract enough water from the root zone. The SPAC system enabled STEMMUS–SCOPE to simulate 30 min LWP. To better detect the response of simulated SIF to simulated LWP, we chose a cloudless day (DOY 199), and a liner relationship between the simulated SIF and LWP was obtained (Fig. 13b). Sun et al. (2016) reported that the SIF–soil moisture–drought relationship depended on variations in both absorbed PAR and fluorescence yield in response to water stress, whereas the LWP can reflect both the effect of absorbed PAR and the soil moisture status. The strong correlation between GPP, LWP, and SIF indicates the potential for using SIF as an effective signal for characterizing the response of photosynthesis to water stress. In the future, more

studies should focus on the measurement of SIF, GPP, and LWP simultaneously for different vegetation types across different environmental conditions (radiation, soil moisture, and CO_2 concentration) to reveal how the water stress affects these relationships.

3.8 Limitations that need to be overcome

The new coupled model notably improved simulations of carbon and water fluxes when vegetation was suffering water stress. However, this study mainly aimed to improve the response of SCOPE to drought by introducing the vertical soil water and root profile. Some critical processes were followed that existed in SCOPE_SM and STEMMUS. As with any model, some modules in STEMMUS–SCOPE, such as plant hydraulics and root growth, could be improved upon in future development.

First, to date many LSMs (e.g., CLM 5, Noah-MP, JULES, and CABLE) have incorporated a state-of-the-art plant hy-

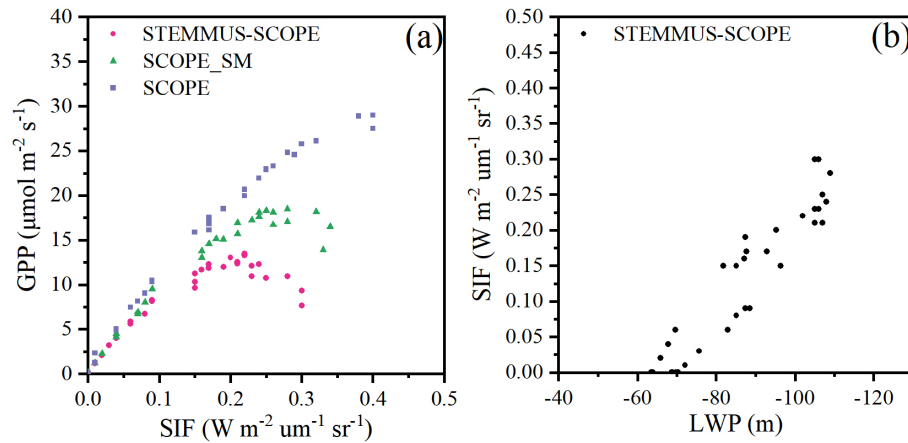


Figure 13. The relationship among gross primary production (GPP), top-of-canopy solar-induced fluorescence (SIF), and leaf water potential (LWP) on DOY 199: **(a)** GPP vs. SIF; **(b)** SIF vs. LWP.

draulics model to replace the conventional empirical plant hydraulic model which was only based on the distribution of SM and the fraction of roots (e.g., CLM 4.5 and CoLM; De Kauwe et al., 2015). Although STEMMUS–SCOPE integrated a 1D root growth model and a relatively novel RWU model, its hydraulics model followed that in SCOPE_SM and ignored the most exciting recent advances in our understanding of plant hydraulics: hydraulic failure due to the loss of hydraulic conductivity owing to embolism and refilling for recovery from xylem embolism (McDowell et al., 2019). Because STEMMUS–SCOPE performed well in maize cropland and grassland, the influence of embolism and refilling on water transfer from the soil through vegetation to the atmosphere cannot be fully detected. The value of using plant water potential instead of soil water potential to constrain model predictions has been demonstrated in many case studies (De Kauwe et al., 2020; Niu et al., 2020; Medlyn et al., 2016; Xu et al., 2016; Williams et al., 1996). Niu et al. (2020) followed the plant hydraulic model developed by Xu et al. (2016) and represented the plant stomatal water stress factor as a function of the plant water storage. CLM 5.0 also introduced a new formulation for WSF, which is based on leaf water potential (ψ_{leaf}) instead of soil water potential (ψ_{soil} ; Kennedy et al., 2019). These new formulations based on plant water potential could offer significant improvements for plant drought responses. Furthermore, STEMMUS–SCOPE presently does not account for plant water storage; this may result in underestimating morning *LE* and overestimating afternoon *LE*. Some field observations have shown that the plant do not immediately respond when soil moisture is enhanced (Mackay et al., 2019), instead there are long lags, which were ignored in this study, between soil water recovery from drought and plant responses to the recovery. The WSF in STEMMUS–SCOPE directly comes from soil moisture and cannot reflect true stomatal response when vegetation is experiencing drought. For example, in

early morning, the low stomatal aperture was induced by low PAR rather than by SM. Consequently, STEMMUS–SCOPE needs to introduce advanced hydraulics after the model has been tested in a wide range of ecosystems, particularly for vegetation exposed to frequent drought cycles or prolonged periods of severe drought events. It is important, however, to note that explicit representations of plant hydraulics require additional model parameters and increase the parameterization burden. This is the most challenging limitation to STEMMUS–SCOPE with respect to incorporating these hydraulics models, and we have chosen a trade-off between mechanism and practicality.

Second, as mentioned above, STEMMUS–SCOPE adapted the macroscopic RWU model and a simplified 1D root growth model in order to save on computational costs, although it predicted maximum root depth well, which is the most critical factor when calculating WSF and RWU. Such a simplification would likely ease the migration of our model into larger-scale models, such as Earth system models. However, STEMMUS–SCOPE oversimplified metabolic processes of the roots, including root exudates, root maintenance respiration, root growth respiration, and root turnover, which are also critical and have been incorporated in Noah-MP (Niu et al., 2020). This simplification could result in uncertainties in modeling the root growth and root water uptake. Meanwhile, there was no validation of the seasonal vertical root length distribution based on in situ observations, which need to be validated in the next step. Furthermore, the model presently does not account for the feedback between hydraulic controls over carbon allocation and the role of root growth on soil–plant hydraulics, which could also be considered in future model development.

4 Conclusions

A fundamental understanding of coupled energy, water, and carbon flux is vital for obtaining information on ecohydrological processes and functioning under climate change. The coupled model, STEMMUS–SCOPE, integrating radiative transfer, photochemistry, energy balance, root system dynamics, and soil moisture and soil temperature dynamics, has been proven to be a practical model to simulate detailed land surface processes such as evapotranspiration and GPP. In the coupled model, STEMMUS could provide the root zone moisture profile to SCOPE, which was used to calculate the water stress factor. On the other hand, SCOPE could provide the net carbon assimilation and soil surface temperature to STEMMUS, which was subsequently used as the top boundary condition and as the input for root growth model. This study explores the role of dynamic root growth in affecting canopy photosynthesis activities, fluorescence emissions, and evapotranspiration, which has not been reported before. The coupled model has been successfully applied in a maize field and a grassland and can be used to describe ET partitioning, canopy photosynthesis, reflectance, and fluorescence emissions. The results show that by considering dynamic root growth and the associated root water uptake, the simulated SIF of the coupled STEMMUS–SCOPE model can respond to water stress, whereas this is not the case for SCOPE_SM.

Through the intercomparison of SCOPE, SCOPE_SM, STEMMUS, and STEMMUS–SCOPE, we concluded that the coupled STEMMUS–SCOPE model can be used to investigate vegetation states under water-stressed conditions and to simultaneously understand the dynamics of soil heat and mass transfer, as well as the root growth. By considering the vertical distribution of soil moisture and the root system, the simulation of water and carbon fluxes, especially when vegetation was suffering moderate water stress, was significantly improved. However, the need remains for further studies to enhance the capacity of STEMMUS–SCOPE with respect to understanding ecosystem functioning. First of all, the estimation of the soil boundary condition, especially during the irrigation period, which has a significant influence on the simulation of soil temperature, requires further consideration. Second, the realism of the present model in modeling the water-stressed SIF will be subject to further studies. Nevertheless, STEMMUS–SCOPE may be used as an effective forward simulator to simulate remote sensing signals and to assimilate remote sensing data, such as solar-induced chlorophyll fluorescence, in order to improve the estimation of water and carbon fluxes. STEMMUS–SCOPE could also be used to investigate regional or global land surface processes, especially in arid and semiarid regions, due to its sensitivity to water-stressed conditions.

Appendix A

A1 Photosynthesis and evapotranspiration under water stress in SCOPE

The C_4 photosynthesis is calculated in the SCOPE model as the minimum of three processes (Collatz et al., 1991, 1992): (1) the carboxylation rate limited by ribulose biphosphate–carboxylase–oxygenase activity (known as rubisco (enzyme) limited), V_c , described in Eq. (A1); (2) the carboxylation rate limited by ribulose 1–5 biphosphate regeneration rate (known as RuBP (electron transport/light) limited), V_e , described in Eq. (A2); and (3) at low CO_2 concentrations, the carboxylation rate limited by intercellular CO_2 partial pressure (p_i), V_s , described in Eq. (A3).

$$V_c = V_{cmax} \cdot WSF \tag{A1}$$

$$V_e = \frac{J - b \pm \sqrt{b^2 - 4ac}}{6} \frac{2a}{2a} \tag{A2}$$

$$V_s = p_i \left(k_p - \frac{L}{p_i} \right) / P \tag{A3}$$

$$A_n = \min(V_c, V_e, V_s) \tag{A4}$$

The C_3 photosynthesis is calculated in the SCOPE model as the minimum of two processes (Farquhar et al., 1980): (1) the carboxylation rate limited by ribulose biphosphate–carboxylase–oxygenase activity (known as rubisco (enzyme) limited), V_c , described in Eq. (A5); and (2) the carboxylation rate limited by ribulose 1–5 biphosphate regeneration rate (known as RuBP (electron transport/light) limited), V_e , described in Eq. (A6).

$$V_c = V_{cmax} \cdot WSF \cdot \frac{C_i - \Gamma^*}{C_i + K_c(1 + \frac{O_i}{K_o})} \tag{A5}$$

$$V_e = \frac{J(C_i - \Gamma^*) - b \pm \sqrt{b^2 - 4ac}}{4(C_i + 2\Gamma^*)} \frac{2a}{2a} \tag{A6}$$

$$A_n = \min(V_c, V_e) \tag{A7}$$

$$C_i = C_a \left(1 - \frac{1}{mRH} \right) \tag{A8}$$

Here, V_{cmax} is the maximum carboxylation rate ($\mu\text{mol m}^{-2} \text{s}^{-1}$), p_i is the intercellular CO_2 partial pressure (Pa), k_p is a pseudo-first-order rate constant for PEP carboxylase with respect to C_i , P is the atmospheric pressure, A_n is the net photosynthesis ($\mu\text{mol m}^{-2} \text{s}^{-1}$), WSF is the total water stress factor, J is the electron transport rate ($\mu\text{mol m}^{-2} \text{s}^{-1}$), C_i is the intercellular CO_2 concentration ($\mu\text{mol m}^{-3}$), C_a is CO_2 concentration in the boundary layer ($\mu\text{mol m}^{-3}$), m is Ball–Berry parameter, and RH is relative humidity at the leaf surface (%).

In addition, leaf stomatal resistance r_c (s m^{-1}) is calculated as

$$r_c = \frac{0.625(C_s - C_i)}{A_n} \frac{\rho_a}{M_a} \frac{10^{12}}{p}, \tag{A9}$$

where ρ_a is specific mass of air (kg m^{-3}), M_a is molecular mass of dry air (g mol^{-1}), and p is atmosphere pressure (hPa).

The calculation of latent heat flux (LE) is as follows:

$$LE = \lambda \frac{(q_i - q_a)}{r_a + r_c}, \tag{A10}$$

where λ is vaporization heat of water (J kg^{-1}), q_i is the humidity in stomata or soil pores (kg m^{-3}), q_a is the humidity above the canopy (kg m^{-3}), r_c is stomatal or soil surface resistance (s m^{-1}), and r_a is aerodynamic resistance (s m^{-1}).

In the study of Bayat et al. (2019), the water stress factor was calculated based on the root zone soil moisture content neglecting the distribution of root length. In this study, the water stress factor considered both root length distribution and water content in root zone. We use a sigmoid formulation rather than the piecewise function by Bayat et al. (2019). The calculations are as follows:

$$WSF = \sum_{i=1}^n RF(i) \cdot WSF(i) \tag{A11}$$

$$WSF(i) = \frac{1}{1 + e^{-100 \cdot \theta_{sat} \left(SM(i) - \frac{\theta_f + \theta_w}{2} \right)}} \tag{A12}$$

where θ_w is the soil water content at wilting point, θ_f is the soil water content at field capacity, θ_{sat} is the saturated soil water content, $WSF(i)$ is the water stress factor at each soil layer, $RF(i)$ is the ratio of root length in soil layer i (its calculation can be found in the Appendix A4), and $SM(i)$ is the soil moisture at each soil layer.

A2 Governing equations in STEMMUS

A2.1 Soil water conservation equation

The soil water conservation equation is as follows:

$$\begin{aligned} \frac{\partial}{\partial t} (\rho_L \theta_L + \rho_V \theta_V) & \tag{A13} \\ &= - \frac{\partial}{\partial z} (q_{Lh} + q_{LT} + q_{La} + q_{Vh} + q_{VT} + q_{Va}) - S \\ &= \rho_L \frac{\partial}{\partial z} \left[K \left(\frac{\partial h}{\partial z} + 1 \right) \right. \\ &\quad \left. + D_{TD} \frac{\partial T_s}{\partial z} + \frac{K}{\gamma_w} \frac{\partial P_g}{\partial z} \right] \\ &\quad + \frac{\partial}{\partial z} \left[D_{Vh} \frac{\partial h}{\partial z} + D_{VT} \frac{\partial T_s}{\partial z} + D_{Va} \frac{\partial P_g}{\partial z} \right] - S, \end{aligned}$$

where ρ_L and ρ_V (kg m^{-3}) are the density of liquid water and water vapor, respectively; q_L and q_V ($\text{m}^3 \text{m}^{-3}$) are the volumetric water content for liquid and water vapor, respectively; $z(m)$ is the vertical space coordinate (positive upwards); S (cm s^{-1}) is the sink term for the root water extraction; K (m s^{-1}) is hydraulic conductivity; h (cm) is the

pressure head; T_s (°C) is the soil temperature; P_g (Pa) is the mixed pore-air pressure; γ_w ($\text{kg m}^{-2} \text{s}^{-2}$) is the specific weight of water; D_{TD} ($\text{kg m}^{-1} \text{s}^{-1} (\text{°C})^{-1}$) is the transport coefficient for adsorbed liquid flow due to the temperature gradient; D_{Vh} ($\text{kg m}^{-2} \text{s}^{-1}$) is the isothermal vapor conductivity; D_{VT} ($\text{kg m}^{-1} \text{s}^{-1} (\text{°C})^{-1}$) is the thermal vapor diffusion coefficient; D_{Va} is the advective vapor transfer coefficient (Zeng et al., 2011a, b); q_{Lh} , q_{LT} , and q_{La} ($\text{kg m}^{-2} \text{s}^{-1}$) are the liquid water fluxes driven by the gradient of matric potential, temperature, and air pressure, respectively; and q_{Vh} , q_{VT} , and q_{Va} ($\text{kg m}^{-2} \text{s}^{-1}$) are the water vapor fluxes driven by the gradient of matric potential, temperature, and air pressure, respectively.

A2.2 Dry-air conservation equation

The dry-air conservation equation is as follows:

$$\frac{\partial}{\partial t} [\varepsilon \rho_{da} (S_a + H_c S_L)] = \frac{\partial}{\partial z} \left[D_e \frac{\partial \rho_{da}}{\partial z} + \rho_{da} \frac{S_a K_g}{\mu_a} \frac{\partial P_g}{\partial z} - H_c \rho_{da} \frac{q_L}{\rho_L} + (\theta_a D_{Vg}) \frac{\partial \rho_{da}}{\partial z} \right], \quad (\text{A14})$$

where ε is the porosity, ρ_{da} (kg m^{-3}) is the density of dry air, $S_a (= 1 - S_L)$ is the degree of air saturation in the soil, $S_L (= \theta_L / \varepsilon)$ is the degree of saturation in the soil, H_c is Henry’s constant, D_e ($\text{m}^2 \text{s}^{-1}$) is the molecular diffusivity of water vapor in soil, K_g (m^2) is the intrinsic air permeability, m_a ($\text{kg m}^{-2} \text{s}^{-1}$) is the air viscosity, q_L ($\text{kg m}^{-2} \text{s}^{-1}$) is the liquid water flux, $\theta_a (= \theta_v)$ is the volumetric fraction of dry air in the soil, and D_{Vg} ($\text{m}^2 \text{s}^{-1}$) is the gas-phase longitudinal dispersion coefficient (Zeng et al., 2011a,b).

A2.3 Energy balance equation

The energy balance equation is as follows:

$$\begin{aligned} \frac{\partial}{\partial t} & \left[(\rho_s \theta_s C_s + \rho_L \theta_L C_L + \rho_V \theta_V C_V + \rho_{da} \theta_a C_a) \right. \\ & \left. \cdot (T_s - T_r) + \rho_V \theta_V L_0 \right] - \rho_L W \frac{\partial \theta_L}{\partial t} \\ & = \frac{\partial}{\partial z} \left(\lambda_{\text{eff}} \frac{\partial T}{\partial z} \right) - \frac{\partial}{\partial z} [q_L C_L (T_s - T_r) \\ & \quad + q_V (L_0 + C_V (T_s - T_r)) + q_a C_a (T_s - T_r)] \\ & \quad - C_L S (T_s - T_r), \end{aligned} \quad (\text{A15})$$

where C_s , C_L , C_V , and C_a ($\text{J kg}^{-1} (\text{°C})^{-1}$) are the specific heat capacities of solids, liquid, water vapor, and dry air, respectively; ρ_s (kg m^{-3}), ρ_L (kg m^{-3}), ρ_V (kg m^{-3}), and ρ_{da} (kg m^{-3}) are the density of solids, liquid water, water vapor, and dry air, respectively; θ_s is the volumetric fraction of solids in the soil; θ_L , θ_V , and θ_a are the volumetric fraction of liquid water, water vapor, and dry air, respectively; T_r (°C)

is the reference temperature; L_0 (J kg^{-1}) is the latent heat of vaporization of water at temperature T_r ; W (J kg^{-1}) is the differential heat of wetting (the amount of heat released when a small amount of free water is added to the soil matrix); λ_{eff} ($\text{W m}^{-1} (\text{°C})^{-1}$) is the effective thermal conductivity of the soil; and q_L , q_V , and q_a ($\text{kg m}^{-2} \text{s}^{-1}$) are the liquid, vapor water and dry air flux, respectively.

A3 Dynamic root growth modeling

A3.1 Root front growth

The depth of the root front is firstly initialized either with the sowing depth for sown crops or with an initial value for transplanted crops or perennial crops. The root front growth stops when it reaches a certain depth of soil or a physical or chemical obstacle preventing root growth, but it also stops when the phenological stopping stage has been reached.

$$\Delta Z = \begin{cases} 0 & T_{\text{air}} < T_{\text{min}} \\ (T_{\text{air}} - T_{\text{min}}) \cdot \text{RGR} & T_{\text{min}} < T_{\text{air}} < T_{\text{max}} \\ (T_{\text{max}} - T_{\text{min}}) \cdot \text{RGR} & T_{\text{max}} < T_{\text{air}} \end{cases} \quad (\text{A16})$$

$$D_Z(t) = D_Z(t - 1) + \Delta Z, \quad (\text{A17})$$

where ΔZ is root front growth at the t th time step, D_Z (cm) is the root zone depth, T_{air} (°C) is air temperature, T_{min} (°C) is the minimum temperature for root growth, T_{max} (°C) is the maximum temperature for root growth, and RGR ($\text{cm } (\text{°C})^{-1} \text{d}^{-1}$) is the root growth rate of root front.

A3.2 Root length growth

In this study, the root distribution in the root zone was realized via simulating the root length growth in each soil layer.

$$\Delta \text{RI}_{\text{tot}} = \frac{A_n \cdot \text{fr}_{\text{root}}}{R_C \cdot R_D \cdot \pi \cdot r_{\text{root}}^2}, \quad (\text{A18})$$

where fr_{root} is the allocation fraction of the net assimilation to root, fr_{root} is assumed as a function of leaf area index (LAI) and root zone water content, A_n is the net assimilation rate ($\mu\text{mol m}^{-2} \text{s}^{-1}$), R_C is the ratio of carbon to dry organic matter in root, R_D is root density (g m^{-3}), r_{root} is the radius of the root, and $\Delta \text{RI}_{\text{tot}}$ (m m^{-3}) is the total root length growth.

The limiting factors for allocation are preliminarily computed, and they account for root zone soil moisture availability, A_W , and light availability, A_L .

$$A_W = \max [0.1, \min (1, \text{WSF})], \quad (\text{A19})$$

where WSF is the averaged soil moisture stress factor in the root zone.

$$A_L = \max \left[0.1, e^{-K_e \text{LAI}} \right], \quad (\text{A20})$$

where $K_e = 0.15$ is a constant light extinction coefficient.

$$fr_{\text{root}} = \max \left[r_{\text{min}}, r_0 \frac{3A_L}{A_L + 2A_W} \right], \quad (\text{A21})$$

where r_{min} ($= 0.15$) is the minimum allocation coefficient to fine roots, and r_0 is a coefficient that indicates the theoretically unstressed allocation to fine roots.

$$\Delta \text{RI}(i) = \Delta \text{RI}_{\text{tot}} \cdot \text{RF}(i), \quad (\text{A22})$$

where $\text{RF}(i)$ is the allocation fraction of root growth length in layer i , and $\Delta \text{RI}(i)$ is the root growth length in layer i .

For $i = 1$ to $n - 1$ ($i = 1$ refers to the top soil layer),

$$\text{RI}_i^t = \text{RI}_i^{t-1} + \Delta \text{RI}(i). \quad (\text{A23})$$

For $i = n$,

$$\text{RI}_i^t = \text{RI}_i^{t-1} + \Delta \text{RI}(i) + \text{RI}_{\text{front}}. \quad (\text{A24})$$

Here, RI_i^t and RI_i^{t-1} are the root length of layer i at time step t and time step $t - 1$, respectively.

$$\text{RF}(i) = \frac{\text{RI}(i)}{\text{RI}_T}, \quad (\text{A25})$$

where RI_T is the total root length in the root zone, and $\text{RI}(i)$ is the root length in soil layer i .

At the root front, the density is imposed and estimated by the parameter L_{v_front} , and the growth in root length depends directly on the root front growth rate ΔZ :

$$\text{RI}_{\text{front}} = L_{v_front} \cdot \Delta Z. \quad (\text{A26})$$

A4 Root water uptake

The equation to calculate root water uptake and transpiration is as follows:

$$\sum_{i=1}^n \frac{\psi_{s,i} - \psi_l}{r_{s,i} + r_{r,i} + r_{x,i}} = \frac{0.622}{P} \frac{\rho_{\text{da}}}{\rho_{\text{v}}} \left(\frac{e_l - e_a}{r_c + r_a} \right) = T, \quad (\text{A27})$$

where $\psi_{s,i}$ is the soil water potential of layer i (pressure head, unit: m), ψ_l is leaf water potential (m), $r_{s,i}$ is the soil hydraulic resistance (s m^{-1}), $r_{r,i}$ is the root resistance to water flow radially across the roots (s m^{-1}), and $r_{x,i}$ is the plant axial resistance to flow from the soil to the leaves (s m^{-1}). e_l and e_a are vapor pressure of leaf and the atmosphere (hPa), respectively, and r_a and r_c are aerodynamic resistance and canopy resistance (s m^{-1}), respectively. ρ_{da} is the density of dry air (kg m^{-3}). ρ_{v} is the density of water vapor. P is the atmospheric pressure (Pa). The ratio of the molar mass of water to air is 0.622.

$\psi_{s,i}$ is described as a function of soil moisture by Van Genuchten (1980), and the relevant parameters are shown in Table B1.

The r_s is calculated by Reid and Huck (1990) as follows:

$$r_s = \frac{1}{B \cdot K \cdot L_v} \cdot \Delta d, \quad (\text{A28})$$

where B is the root length activity factor, K is hydraulic conductivity of soil (m s^{-1}), L_v is root length density (mm^{-3}), and Δd is the thickness of the soil layer (m). B is calculated as

$$B = \frac{2\pi}{\ln \left[(\pi R_D)^{-1/2} / r_{\text{root}} \right]}, \quad (\text{A29})$$

where r_{root} is root radius (m).

The r_r is estimated as (Reid and Huck, 1990) follows:

$$r_r = \frac{P_r (\theta_{\text{sat}} / \theta)}{L_v \Delta d}, \quad (\text{A30})$$

where P_r is root radial resistivity (s m^{-1}).

The xylem resistance r_x is estimated by Klepper et al. (1983):

$$r_x = \frac{P_a Z_{\text{mid}}}{0.5 f L_v}, \quad (\text{A31})$$

where P_a is root axial resistivity (s m^{-3}), Z_{mid} is the depth of the midpoint of the soil layer, and f is a fraction defined for a specific depth as the number of roots that connect directly to the stem base to total roots crossing a horizontal plane at that depth. We can consider it equal to 0.22 based on Klepper et al. (1983).

The updated root water uptake term is

$$S_i = \frac{\psi_{s,i} - \psi_l}{r_{s,i} + r_{r,i} + r_{x,i}}. \quad (\text{A32})$$

In contrast to other studies that need to calculate the compensatory water uptake and hydraulic redistribution after calculating the standard water uptake of each soil layer, the sink term in this study is calculated by a physically based model that contains the effect of root resistance and soil hydraulic resistance rather than only considering the root fraction; thus, the compensatory water uptake and hydraulic redistribution have been considered when calculating the sink term.

Appendix B

Table B1. List of parameters and values used in this study (all the parameters were classified as air, canopy, root, and soil).

Symbol	Description	Unit	Value	
			Maize	Grass
Aerodynamic				
aPAR	Absorbed photosynthetically active radiation	$\mu\text{mol m}^{-2} \text{s}^{-1}$		
e_a	Air vapor pressure	Pa		
e_l	Vapor pressure of leaf	hPa		
P	Air pressure	Pa		
q_a	Humidity above the canopy	kg m^{-3}		
q_l	Humidity in stomata	kg m^{-3}		
r_a	Aerodynamic resistance	s m^{-1}		
RH	Relative humidity	%		
R_{li}	Incoming longwave radiation	W m^{-2}		
R_{in}	Incoming shortwave radiation	W m^{-2}		
R_n	Net radiation	W m^{-2}		
T_{air}	Air temperature	$^{\circ}\text{C}$		
u	Wind speed	m s^{-1}		
VPD	Vapor pressure deficit	hPa		
Canopy				
A_n	Net assimilation rate	$\mu\text{mol m}^{-2} \text{s}^{-1}$		
C_a	CO_2 concentration in the boundary layer	$\mu\text{mol m}^{-3}$		
C_{ab}	Leaf chlorophyll content	$\mu\text{g cm}^{-2}$	80	0.374–50.45
C_{ca}	Leaf carotenoid content	$\mu\text{g cm}^{-2}$	20	$0.25 \cdot C_{ab}$
C_w	Leaf water content	g cm^{-2}	0.009	0.02
C_{dm}	Leaf dry matter content	g cm^{-2}	0.012	0.015
C_s	Senescent material content		0	0
DOY	Day of year	d		
ET	Evapotranspiration	mm d^{-1}		
GPP	Gross primary production	$\text{g C m}^{-2} \text{d}^{-1}$		
h_c	Canopy height	m	0–1.95	0.55
H	Sensible heat flux	W m^{-2}		
J	Electron transport rate	$\mu\text{mol m}^{-2} \text{s}^{-1}$		
K_e	Light extinction coefficient		0.15	0.15
k_p	A pseudo-first-order rate constant for PEP carboxylase			
LAI	Leaf area index	$\text{m}^2 \text{m}^{-2}$	0–4.39	0.745–2.03
LIDF	Leaf inclination distribution function		–1, 0	0.08, –0.15
LE	Latent heat flux	W m^{-2}		
LE_c	Latent heat flux of canopy	W m^{-2}		
m	Ball–Berry stomatal conductance parameter	4	10	
NEE	Net ecosystem exchange	$\text{g C m}^{-2} \text{d}^{-1}$		
p_i	Intercellular CO_2 partial pressure	Pa		
r_c	Canopy resistance	s m^{-1}		
Re	Ecosystem respiration	$\text{g C m}^{-2} \text{d}^{-1}$		
T	Transpiration	mm d^{-1}		
T_c	Vegetation temperature	$^{\circ}\text{C}$		
T_{ch}	Leaf temperature (shaded leaves)	$^{\circ}\text{C}$		
T_{cu}	Leaf temperature (sunlit leaves)	$^{\circ}\text{C}$		
uWUE _p	Potential water use efficiency	$\text{g C hPa}^{0.5} (\text{kg H}_2\text{O})^{-1}$		
uWUE	Water use efficiency	$\text{g C hPa}^{0.5} (\text{kg H}_2\text{O})^{-1}$		
V_{cmax}	Maximum carboxylation rate	$\mu\text{mol m}^{-2} \text{s}^{-1}$	50	10.7–100.3
ψ_{leaf}	Leaf water potential	m		

Table B1. Continued.

Symbol	Description	Unit	Value	
Root			Maize	Grass
A_W	Root zone soil moisture availability			
A_L	Light availability			
B	Root length activity factor			
D_Z	Root zone depth	cm		
f	A fraction defined for a specific depth as the number of roots that connect directly to the stem base to total roots crossing a horizontal plane at that depth		0.22	0.22
fr_{root}	Allocation fraction of net assimilation to root			
P_a	Root axial resistivity	s m^{-3}	0.65×10^{12}	2×10^{12}
P_r	Root radial resistivity	s m^{-1}	1×10^{10}	1.2×10^{11}
$RF(i)$	The allocation fraction of root growth length in layer i			
RI_T	Total root length in root zone	mm^{-2}		
RI_t^i	Root length of layer i at time step t	mm^{-2}		
RI_{t-1}^i	Root length of layer i at time step $t-1$	mm^{-2}		
$RI(i)$	Root length in soil layer i	mm^{-2}		
RI_{front}	Growth at the root front	mm^{-2}		
RGR	Root growth rate of front	$\text{cm} (\text{°C}) \text{d}^{-1}$	0.096	0.072
R_D	Root density	g m^{-3}	250000	250000
L_v	Root length density	mm^{-3}		
L_{v_front}	Root density at the root front	mm^{-3}	1000	150
r_{min}	The minimum allocation coefficient to fine roots		0.15	0.15
r_0	Coefficient of theoretically unstressed allocation to fine roots		0.3	0.3
r_{root}	Radius of the root	m	0.15×10^{-3}	1.5×10^{-3}
$r_{x,i}$	Plant axial resistance to flow from the soil to the leaves	s		
$r_{r,i}$	Resistance to water flow radially across the roots	s		
$r_{s,i}$	Soil hydraulic resistance	s		
R_C	Ratio of carbon to dry organic matter in root	kg kg^{-1}	0.488	0.488
RWU	Root water uptake	ms^{-1}		
$RF(i)$	The ratio of root length in soil layer i			
T_{min}	Minimum temperature of root growth	°C	10	0
T_{max}	Maximum temperature of root growth	°C	40	40
ΔZ	Root front growth at t th step	cm		
ΔRI_{tot}	Total root length growth	m		
$\Delta RI(i)$	The root growth length in layer i	m		
C_s	Specific heat capacities of solids	$\text{J kg}^{-1} (\text{°C})^{-1}$		
C_L	Specific heat capacities of liquid	$\text{J kg}^{-1} (\text{°C})^{-1}$	4.186×10^3	4.186×10^3
C_V	Specific heat capacities of water vapor	$\text{J kg}^{-1} (\text{°C})^{-1}$	1.870×10^3	1.870×10^3
C_a	Specific heat capacities of dry air	$\text{J kg}^{-1} (\text{°C})^{-1}$	1.255×10^{-3}	1.255×10^{-3}
D_{TD}	Transport coefficient for absorbed liquid flow due to temperature gradient	$\text{kg m}^{-1} \text{s}^{-1} (\text{°C})^{-1}$		
D_{Vh}	Isothermal vapor conductivity	$\text{kg m}^{-2} \text{s}^{-1}$		
D_{VT}	Thermal vapor diffusion coefficient	$\text{kg m}^{-1} \text{s}^{-1} (\text{°C})^{-1}$		
D_{Va}	Advective vapor transfer coefficient	$\text{kg m}^{-2} \text{s}^{-1}$		
D_{Vg}	Gas-phase longitudinal dispersion coefficient	$\text{m}^2 \text{s}^{-1}$		
D_e	Molecular diffusivity of water vapor in soil	$\text{m}^2 \text{s}^{-1}$		
E	Soil evaporation	mm		
G	Soil heat flux	W m^{-2}		
h	Soil matric potential	cm		
H_c	Henry's constant		0.02	0.02
K	Hydraulic conductivity	ms^{-1}		
K_g	Intrinsic air permeability	m^2		
K_s	Saturation hydraulic conductivity	cmd^{-1}	18	10

Table B1. Continued.

Symbol	Description	Unit	Value	
			Maize	Grass
Soil				
LE_s	Latent heat flux of soil	$W m^{-2}$		
L_0	Latent heat of vaporization of water temperature T_r	$J kg^{-1}$	2 497 909	2 497 909
m_a	Air viscosity	$kg m^{-1} s^{-1}$	1.846×10^{-5}	1.846×10^{-5}
n	Soil-dependent parameter		1.41	1.50
P_g	Mixed pore-air pressure	Pa		
q_L	Liquid water flux	$kg m^{-2} s^{-1}$		
q_{Lh}	Liquid water flux driven by the gradient of matric potential	$kg m^{-2} s^{-1}$		
q_{LT}	Liquid water flux driven by the gradient of temperature	$kg m^{-2} s^{-1}$		
q_{La}	Liquid water flux driven by the gradient of air pressure	$kg m^{-2} s^{-1}$		
q_V	Water vapor flux	$kg m^{-2} s^{-1}$		
q_{Vh}	Water vapor flux driven by the gradient of matric potential	$kg m^{-2} s^{-1}$		
q_{VT}	Water vapor flux driven by the gradient of temperature	$kg m^{-2} s^{-1}$		
q_{Va}	Water vapor flux driven by the gradient of air pressure	$kg m^{-2} s^{-1}$		
q_a	Dry-air flux	$kg m^{-2} s^{-1}$		
S	Sink term for the root water extraction	$cm s^{-1}$		
S_a	Degree of air saturation in the soil			
S_L	Degree of saturation in the soil			
$SM(i)$	The soil moisture at a specific soil layer	$m^3 m^{-3}$		
T_s	Soil temperature	$^{\circ}C$		
T_{s0}	Soil surface temperature	$^{\circ}C$		
T_r	Reference temperature	$^{\circ}C$	20	20
W	Differential heat of wetting	$J kg^{-1}$	1.001×10^3	1.001×10^3
WSF	Total water stress factor			
WSF(i)	Water stress factor at a specific soil layer			
Z_{mid}	The depth of the midpoint of soil layer	m		
Δd	Thickness of the soil layer	m		
α	Soil-dependent parameter	m^{-1}	0.45	0.166
θ_{sat}	Saturated water content	$m^3 m^{-3}$	0.42	0.38
θ_f	Field capacity	$m^3 m^{-3}$	0.272	0.24
θ_w	Wilting point	$m^3 m^{-3}$	0.10	0.03
θ_r	Residual water content	$m^3 m^{-3}$	0.0875	0.0008
θ	Volumetric soil water content	$m^3 m^{-3}$		
θ_L	Volumetric moisture content	$m^3 m^{-3}$		
θ_V	Volumetric vapor content	$m^3 m^{-3}$		
θ_s	Volumetric fraction of solids in the soil	$m^3 m^{-3}$		
θ_a	Volumetric fraction of dry air in the soil	$m^3 m^{-3}$		
$\psi_{s,i}$	Soil water potential of layer i	m		
ψ_{soil}	Soil water potential	m		
λ_{eff}	Effective thermal conductivity of the soil	$W m^{-1} (^{\circ}C)^{-1}$		
γ_w	Specific weight of water	$kg m^{-2} s^{-2}$		
ρ_{da}	Density of dry air	$kg m^{-3}$		
ρ_V	Density of vapor	$kg m^{-3}$		
ρ_L	Density of liquid water	$kg m^{-3}$	1	1
ρ_s	Density of solids	$kg m^{-3}$		
ε	Soil porosity	$m^3 m^{-3}$	0.50	0.50

Code and data availability. The development and validation of STEMMUS–SCOPE in this paper were conducted in MATLAB R2016a. The exact version of the model used to produce the results employed in this paper is archived on Zenodo (<https://doi.org/10.5281/zenodo.3839092>, Wang et al., 2020). The original source of the SCOPE model and STEMMUS model was obtained from Van der Tol et al. (2009) and Zeng et al. (2011a, b), respectively. The tower-based eddy-covariance measurements used for model validation were provided by the authors for the Yangling station, China (<https://doi.org/10.4121/uuid:aa0ed483-701e-4ba0-b7b0-674695f5f7a7>, Wang et al., 2019), and were obtained from the FLUXNET2015 Dataset and PLUMBER2 program for the Vaira Ranch (US-Var) FLUXNET site.

Author contributions. YW, YZ, HC, and ZS designed the study. YW developed the code, conducted the analysis, and wrote the paper. YW and HC collected and shared their eddy-covariance measurements for the purpose of model validation. All authors discussed, commented, and contributed to the revisions and final version of the article.

Competing interests. The authors declare that they have no conflict of interest.

Acknowledgements. This work was supported by the National Natural Science Foundation of China (grant nos. 51879223 and 41971033); the National Key Research and Development Program of China (grant no. 2016YFC0400201); the Fundamental Research Funds for the Central Universities, CHD (grant no. 300102298307); and the China Scholarship Council. Peiqi Yang was supported by the Netherlands Organization for Scientific Research (grant no. ALWGO.2017.018).

Financial support. This research has been supported by the National Natural Science Foundation of China (grant no. 51879223).

Review statement. This paper was edited by Hisashi Sato and reviewed by three anonymous referees.

References

- Amato, M. and Ritchie, J. T.: Spatial distribution of roots and water uptake of maize (*Zea mays* L.) as affected by soil structure, *Crop Sci.*, 42, 773–780, <https://doi.org/10.2135/cropsci2002.7730>, 2002.
- Amenu, G. G. and Kumar, P.: A model for hydraulic redistribution incorporating coupled soil-root moisture transport, *Hydrol. Earth Syst. Sci.*, 12, 55–74, <https://doi.org/10.5194/hess-12-55-2008>, 2008.
- Aston, M. and Lawlor, D. W.: The relationship between transpiration, root water uptake, and leaf water potential, *J. Exp. Bot.*, 30, 169–181, <https://doi.org/10.1093/jxb/30.1.169>, 1979.
- Bayat, B., Van der Tol, C., and Verhoef, W.: Integrating satellite optical and thermal infrared observations for improving daily ecosystem functioning estimations during a drought episode, *Remote Sens. Environ.*, 209, 375–394, <https://doi.org/10.1016/j.rse.2018.02.027>, 2018.
- Bayat, B., Van der Tol, C., Yang, P., and Verhoef, W.: Extending the SCOPE model to combine optical reflectance and soil moisture observations for remote sensing of ecosystem functioning under water stress conditions, *Remote Sens. Environ.*, 221, 286–301, <https://doi.org/10.1016/j.rse.2018.11.021>, 2019.
- Beaudoin, N., Mary, B., Launay, M., and Brisson, N.: Conceptual basis, formalisations and parameterization of the STICS crop model, Editions Quae, Versailles Cedex, France, 2009.
- Bingham, I. J. and Wu, L.: Simulation of wheat growth using the 3D root architecture model SPACSYS: validation and sensitivity analysis, *Eur. J. Agron.*, 34, 181–189, <https://doi.org/10.1016/j.eja.2011.01.003>, 2011.
- Caldwell, M. M., Dawson, T. E., and Richards, J. H.: Hydraulic lift: consequences of water efflux from the roots of plants, *Oecologia*, 113, 151–161, <https://doi.org/10.1007/s004420050363>, 1998.
- Camargo, G. and Kemanian, A.: Six crop models differ in their simulation of water uptake, *Agr. Forest Meteorol.*, 220, 116–129, <https://doi.org/10.1016/j.agrformet.2016.01.013>, 2016.
- Chassot, A., Stamp, P., and Richner, W.: Root distribution and morphology of maize seedlings as affected by tillage and fertilizer placement, *Plant Soil*, 231, 123–135, <https://doi.org/10.1023/A:1010335229111>, 2001.
- Collatz, G. J., Ball, J. T., Grivet, C., and Berry, J. A.: Physiological and environmental regulation of stomatal conductance, photosynthesis and transpiration, *Agr. Forest Meteorol.*, 54, 107–136, [https://doi.org/10.1016/0168-1923\(91\)90002-8](https://doi.org/10.1016/0168-1923(91)90002-8), 1991.
- Collatz, G. J., Ribas-Carbo, M., Berry, J. A.: Coupled photosynthesis-stomatal conductance model for leaves of C4 plants, *Aust. J. Plant Physiol.*, 19, 519–538, 1992.
- Couvreur, V., Vanderborght, J., and Javaux, M.: A simple three-dimensional macroscopic root water uptake model based on the hydraulic architecture approach, *Hydrol. Earth Syst. Sci.*, 16, 2957–2971, <https://doi.org/10.5194/hess-16-2957-2012>, 2012.
- De Kauwe, M. G., Zhou, S.-X., Medlyn, B. E., Pitman, A. J., Wang, Y.-P., Duursma, R. A., and Prentice, I. C.: Do land surface models need to include differential plant species responses to drought? Examining model predictions across a mesic-xeric gradient in Europe, *Biogeosciences*, 12, 7503–7518, <https://doi.org/10.5194/bg-12-7503-2015>, 2015.
- De Kauwe, M. G., Medlyn, B. E., Ukkola, A. M., Mu, M., Sabot, M. E., Pitman, A. J., Meir, P., Cernusak, L., Rifai, S. W., Choat, B., Tissue, D. T., Blackman, C. J., Li, X., Roderick, M., and Briggs, P. R.: Identifying areas at risk of drought-induced tree mortality across SouthEastern Australia, *Glob. Change Biol.*, 26, 5716–5733, <https://doi.org/10.1111/gcb.15215>, 2020.
- Deng, Z., Guan, H., Hutson, J., Forster, M. A., Wang, Y., and Simmons, C. T.: A vegetation focused soil-plant-atmospheric continuum model to study hydrodynamic soil-plant water relations, *Water Resour. Res.*, 53, 4965–4983, <https://doi.org/10.1002/2017WR020467>, 2017.
- Elfving, D. C., Kaufmann, M. R., and Hall, A. E.: Interpreting leaf water potential measurements with a model of the soil-plant-atmosphere continuum, *Physiol. Plant.*, 27, 161–168, <https://doi.org/10.1111/j.1399-3054.1972.tb03594.x>, 1972.

- Eller, C. B., Rowland, L., Mencuccini, M., Rosas, T., Williams, K., Harper, A., Medlyn, B., Wagner, Y., Klein, T., Teodoro, G., Oliveira, R., Matos, I., Rosado, B. H. P., Fuchs, K., Wohlfahrt, G., Montagnani, L., Meir, P., Sitch, S., and Cox, P.: Stomatal optimization based on xylem hydraulics (SOX) improves land surface model simulation of vegetation responses to climate, *New Phytol.*, 226, 1622–1637, <https://doi.org/10.1111/nph.16419>, 2020.
- Espeleta, J., West, J., and Donovan, L.: Species-specific patterns of hydraulic lift in co-occurring adult trees and grasses in a sandhill community, *Oecologia*, 138, 341–349, <https://doi.org/10.1007/s00442-004-1539-x>, 2004.
- Fan, X., Hu, H., Huang, G., Huang, F., Li, Y., and Palta, J.: Soil inoculation with *Burkholderia* sp. LD-11 has positive effect on water-use efficiency in inbred lines of maize, *Plant Soil*, 390, 337–349, <https://doi.org/10.1007/s11104-015-2410-z>, 2015.
- Farquhar, G. D., von Caemmerer, S., and Berry, J. A.: A biochemical model of photosynthetic CO₂ assimilation in leaves of C3 species, *Planta*, 149, 78–90, <https://doi.org/10.1007/bf00386231>, 1980.
- Fu, C., Wang, G., Goulden, M. L., Scott, R. L., Bible, K., and G. Cardon, Z.: Combined measurement and modeling of the hydrological impact of hydraulic redistribution using CLM4.5 at eight AmeriFlux sites, *Hydrol. Earth Syst. Sci.*, 20, 2001–2018, <https://doi.org/10.5194/hess-20-2001-2016>, 2016.
- Guo, Y.: Simulation of water transport in the soil-plant-atmosphere system, Iowa State University, USA, <https://doi.org/10.31274/rtid-180813-9473>, 1992.
- Jarvis, N. J.: Simple physics-based models of compensatory plant water uptake: concepts and eco-hydrological consequences, *Hydrol. Earth Syst. Sci.*, 15, 3431–3446, <https://doi.org/10.5194/hess-15-3431-2011>, 2011.
- Jones, J. W., Hoogenboom, G., Porter, C. H., Boote, K. J., Batchelor, W. D., Hunt, L., Wilkens, P. W., Singh, U., Gijsman, A. J., and Ritchie, J. T.: The DSSAT cropping system model, *Eur. J. Agron.*, 18, 235–265, [https://doi.org/10.1016/s1161-0301\(02\)00107-7](https://doi.org/10.1016/s1161-0301(02)00107-7), 2003.
- Keating, B. A., Carberry, P. S., Hammer, G. L., Probert, M. E., Robertson, M. J., Holzworth, D., Huth, N. I., Hargreaves, J. N., Meinke, H., and Hochman, Z.: An overview of APSIM, a model designed for farming systems simulation, *Eur. J. Agron.*, 18, 267–288, [https://doi.org/10.1016/s1161-0301\(02\)00108-9](https://doi.org/10.1016/s1161-0301(02)00108-9), 2003.
- Kennedy, D., Swenson, S., Oleson, K. W., Lawrence, D. M., Fisher, R. A., da Costa, A., and Gentine, P.: Implementing plant hydraulics in the community land model, version 5, *J. Adv. Model. Earth Sy.*, 11, 485–513, <https://doi.org/10.1029/2018MS001500>, 2019.
- Klepper, B., Rickman, R. W., and Taylor, H. M.: Farm management and the function of field crop root systems, *Agric. Water Manage.*, 7, 115–141, [https://doi.org/10.1016/0378-3774\(83\)90078-1](https://doi.org/10.1016/0378-3774(83)90078-1), 1983.
- Krinner, G., N. Viovy, de Noblet-Ducoudre, N., Ogee, J., Polcher, J., Friedlingstein, P., Ciais, P., Sitch, S., and Prentice, I. C.: A dynamic global vegetation model for studies of the coupled atmosphere-biosphere system, *Global Biogeochem. Cy.*, 19, GB1015, <https://doi.org/10.1029/2003GB002199>, 2005.
- Lawrence, D., Fisher, R., Koven, C., Oleson, K., Swenson, S., and Vertenstein, M.: Technical Description of version 5.0 of the Community LandModel (CLM), 2020.
- Leitner, D., Klepsch, S., Bodner, G., and Schnepf, A.: A dynamic root system growth model based on L-Systems, *Plant Soil*, 332, 177–192, <https://doi.org/10.1007/s11104-010-0284-7>, 2010.
- Mackay, D. S., Savoy, P. R., Grossiord, C., Tai, X., Oleban, J., Wang, D., McDowell, N., Adams, H., Sperry, J. S.: Conifers depend on established roots during drought: results from a coupled model of carbon allocation and hydraulics, *New Phytol.*, 225, 679–692, <https://doi.org/10.1111/nph.16043>, 2019.
- Martineau, E., Domec, J.-C., Bosc, A., Denoroy, P., Fandino, V. r.A., Lavres Jr., J., and Jordan-Meille, L.: The effects of potassium nutrition on water use in field-grown maize (*Zea mays* L.), *Environ. Exp. Bot.*, 134, 62–71, <https://doi.org/10.1016/j.envexpbot.2016.11.004>, 2017.
- Medlyn, B. E., Kauwe, M. G. D., and Duursma, R. A.: New developments in the effort to model ecosystems under water stress, *New Phytol.*, 212, 5–7, <https://doi.org/10.1111/nph.14082>, 2016.
- McDowell, N. G., Brodrigg, T. J., and Nardini, A.: Hydraulics in the 21st century, *New Phytol.*, 224, 537–542, <https://doi.org/10.1111/nph.16151>, 2019.
- Mohammed, G. H., Colombo, R., Middleton, E. M., Rascher, U., Van der Tol, C., Nedbal, L., Goulas Y., Perez-Priego, O., Damm A., Meroni M., Joiner J., Cogliati S., Verhoef W., Malenovskiy Z., Gastellu-Etchegorry J., Miller, J., Guanter, L., Moreno, J., Berry, J., Frankenberg, C., Zarco-Tejada, P. J.: Remote sensing of solar-induced chlorophyll fluorescence (SIF) in vegetation: 50 years of progress, *Remote Sens. Environ.*, 231, 111177, <https://doi.org/10.1016/j.rse.2019.04.030>, 2019.
- Ning, P., Li, S., White, P. J., and Li, C.: Maize varieties released in different eras have similar root length density distributions in the soil, which are negatively correlated with local concentrations of soil mineral nitrogen, *PLOS ONE*, 10, e0121892, <https://doi.org/10.1371/journal.pone.0121892>, 2015.
- Niu, G., Fang, Y., Chang, L., Jin, J., Yuan, H., and Zeng, X.: Enhancing the Noah-MP ecosystem response to droughts with an explicit representation of plant water storage supplied by dynamic root water uptake, *J. Adv. Model. Earth Syst.*, 12, e2020MS002062, <https://doi.org/10.1029/2020MS002062>, 2020.
- O’Toole, J. C. and Cruz, R. T.: Response of leaf water potential, stomatal resistance, and leaf rolling to water stress, *Plant Physiol.*, 65, 428–432, <https://doi.org/10.1104/pp.65.3.428>, 1980.
- Oikeh, S., Kling, J., Horst, W., Chude, V., and Carsky, R.: Growth and distribution of maize roots under nitrogen fertilization in plinthite soil, *Field Crop. Res.*, 62, 1–13, [https://doi.org/10.1016/s0378-4290\(98\)00169-5](https://doi.org/10.1016/s0378-4290(98)00169-5), 1999.
- Peng, Y., Yu, P., Zhang, Y., Sun, G., Ning, P., Li, X., and Li, C.: Temporal and spatial dynamics in root length density of field-grown maize and NPK in the soil profile, *Field Crop. Res.*, 131, 9–16, <https://doi.org/10.1016/j.fcr.2012.03.003>, 2012.
- Qin, R., Stamp, P., and Richner, W.: Impact of tillage on maize rooting in a Cambisol and Luvisol in Switzerland, *Soil Till. Res.*, 85, 50–61, <https://doi.org/10.1016/j.still.2004.12.003>, 2006.
- Reichstein, M., Falge, E., Baldocchi, D., Papale, D., Aubinet, M., Berbigier, P., Bernhofer, C., Buchmann, N., Gilmanov, T., and Granier, A.: On the separation of net ecosystem exchange into assimilation and ecosystem respiration: review

- and improved algorithm, *Glob. Change Biol.*, 11, 1424–1439, <https://doi.org/10.1111/j.1365-2486.2005.001002.x>, 2005.
- Reid, J. B. and Huck, M. G.: Diurnal variation of crop hydraulic resistance: a new analysis, *Agron. J.*, 82, 827–834, [https://doi.org/10.1016/0378-3774\(90\)90029-X](https://doi.org/10.1016/0378-3774(90)90029-X), 1990.
- Richards, J. H. and Caldwell, M. M.: Hydraulic lift: substantial nocturnal water transport between soil layers by *Artemisia tridentata* roots, *Oecologia*, 73, 486–489, <https://doi.org/10.1007/bf00379405>, 1987.
- Robertson, M., Fukai, S., Hammer, G., and Ludlow, M.: Modelling root growth of grain sorghum using the CERES approach, *Field Crop. Res.*, 33, 113–130, [https://doi.org/10.1016/0378-4290\(93\)90097-7](https://doi.org/10.1016/0378-4290(93)90097-7), 1993.
- Ryel, R., Caldwell, M., Yoder, C., Or, D., and Leffler, A.: Hydraulic redistribution in a stand of *Artemisia tridentata*: evaluation of benefits to transpiration assessed with a simulation model, *Oecologia*, 130, 173–184, <https://doi.org/10.1007/s004420100794>, 2002.
- Schroder, J., Groenwold, J., and Zaharieva, T.: Soil mineral nitrogen availability to young maize plants as related to root length density distribution and fertilizer application method, *NJAS-Wagen, J. Life Sci.*, 44, 209–225, 1996.
- Seneviratne, S. I., Corti, T., Davin, E. L., Hirschi, M., Jaeger, E. B., Lehner, I., Orlowsky, B., and Teuling, A. J.: Investigating soil moisture–climate interactions in a changing climate: a review, *Earth-Sci. Rev.*, 99, 125–161, <https://doi.org/10.1016/j.earscirev.2010.02.004>, 2010.
- Shan, N., Ju, W., Migliavacca, M., Martini, D., Guanter, L., and Chen, J. M., Goulas, Y., and Zhang, Y.: Modeling canopy conductance and transpiration from solar-induced chlorophyll fluorescence, *Agr. Forest Meteorol.*, 268, 189–201, <https://doi.org/10.1016/j.agrformet.2019.01.031>, 2019.
- Stöckle, C. O., Donatelli, M., and Nelson, R.: CropSyst, a cropping systems simulation model, *Eur. J. Agron.*, 18, 289–307, [https://doi.org/10.1016/S1161-0301\(02\)00109-0](https://doi.org/10.1016/S1161-0301(02)00109-0), 2003.
- Sulis, M., Couvreur, V., Keune, J., Cai, G., Trebs, I., Junk, J., Junk, J., Shrestha, P., Simmer, C., Kollet, S. J., Vereecken, H., Vanderborght, J.: Incorporating a root water uptake model based on the hydraulic architecture approach in terrestrial systems simulations, *Agr. Forest Meteorol.*, 269270, 28–45, <https://doi.org/10.1016/j.agrformet.2019.01.034>, 2019.
- Sun, Y., Fu, R., Dickinson, R., Joiner, J., Frankenberg, C., Gu, L., Xia, Y., and Fernando, N.: Drought onset mechanisms revealed by satellite solar-induced chlorophyll fluorescence: insights from two contrasting extreme events, *J. Geophys. Res.-Biogeo.*, 120, 2427–2440, <https://doi.org/10.1002/2015JG003150>, 2016.
- Supit, I., Hooijer, A., and Van Diepen, C.: System description of the WOFOST 6.0 crop simulation model implemented in CGMS, vol. 1: Theory and Algorithms, Joint Research Centre, Commission of the European Communities, 146, EUR 15956, 1994.
- Van Dam, J. C.: Field-Scale Water Flow and Solute Transport. SWAP ModelConcepts, Parameter Estimation and Case Studies, Wageningen University, Wageningen, the Netherlands, 167 pp., 2000.
- van der Tol, C., Verhoef, W., Timmermans, J., Verhoef, A., and Su, Z.: An integrated model of soil–canopy spectral radiances, photosynthesis, fluorescence, temperature and energy balance, *Biogeosciences*, 6, 3109–3129, <https://doi.org/10.5194/bg-6-3109-2009>, 2009.
- Van der Tol, C., Berry, J., Campbell, P., Rascher, U.: Models of fluorescence and photosynthesis for interpreting measurements of solar-induced chlorophyll fluorescence, *J. Geophys. Res.-Biogeo.*, 119, 2312–2327, <https://doi.org/10.1002/2014JG002713>, 2014.
- Van Genuchten, M. T.: A closed-form equation for predicting the hydraulic conductivity of unsaturated soils, *Soil Sci. Soc. Am. J.*, 44, 892–898, <https://doi.org/10.2136/sssaj1980.03615995004400050002x>, 1980.
- Wang, E. and Smith, C. J.: Modelling the growth and water uptake function of plant root systems: a review, *Aust. J. Agr. Res.*, 55, 501–523, <https://doi.org/10.1071/ar03201>, 2004.
- Wang, Y., Cai, H. J., Zeng, Y. J., Su, Z., and Yu, L. Y.: Data underlying the research on Seasonal and interannual variation in evapotranspiration, energy flux, and Bowen ratio over a dry semi-humid cropland in Northwest China, 4TU, Centre for Research Data, Dataset, <https://doi.org/10.4121/uuid:aa0ed483-701e-4ba0-b7b0-674695f5f7a7>, 2019.
- Wang, Y., Cai, H. J., Yu, L. Y., Peng, X. B., Xu, J. T., and Wang, X. W.: Evapotranspiration partitioning and crop coefficient of maize in dry semi-humid climate regime, *Agric. Water Manag.*, 236, 106164, <https://doi.org/10.1016/j.agwat.2020.106164>, [preprint], 2020a.
- Wang, Y., Zeng, Y. J., Yu, L. Y., Yang, P., Van der Tol, C., Su, Z., and Cai, H. J.: Integrated Modeling of Photosynthesis and Transfer of Energy, Mass and Momentum (SCOPE_STEMMUS v1.0), Zenodo, <https://doi.org/10.5281/zenodo.3839092>, 2020b.
- Wiesler, F. and Horst, W.: Root growth and nitrate utilization of maize cultivars under field conditions, *Plant Soil*, 163, 267–277, <https://doi.org/10.1007/bf00007976>, 1994.
- Williams, J., Jones, C., Kiniry, J., and Spanel, D. A.: The EPIC crop growth model, *T. ASAE*, 32, 497–511, <https://doi.org/10.13031/2013.31032>, 1989.
- Williams, J. R., Gerik, T., Francis, L., Greiner, J., Magre, M., Meinardus, A., Steglich, E., and Taylor, R.: EPIC – Environmental Policy Integrated Climate Model, UsersManual version 0810, Blackland Research and Extension Center, Texas A&M AgriLife, Temple, TX, 2014.
- Williams, M., Rastetter, E. B., Fernandes, D. N., Goulden, M. L., Wofsy, S. C., Shaver G. R., Melillo J. M., Munger, J. W., Fan, S. M., and Nadelhoffer, K. J.: Modelling the soil–plant–atmosphere continuum in a *Quercus-Acer* stand at Harvard Forest: the regulation of stomatal conductance by light, nitrogen and soil/plant hydraulic properties, *Plant Cell Environ.*, 19, 911–927, <https://doi.org/10.1111/j.1365-3040.1996.tb00456.x>, 1996.
- Wu, L., McGechan, M., Watson, C., and Baddeley, J.: Developing existing plant root system architecture models to meet future agricultural challenges, *Adv. Agron.*, 85, 85004–85001, [https://doi.org/10.1016/S0065-2113\(04\)85004-1](https://doi.org/10.1016/S0065-2113(04)85004-1), 2005.
- Xu, L. and Baldocchi, D. D.: Seasonal trends in photosynthetic parameters and stomatal conductance of blue oak (*Quercus douglasii*) under prolonged summer drought and high temperature, *Tree Physiol.*, 23, 865–877, <https://doi.org/10.1093/treephys/23.13.865>, 2003.
- Xu, X., Medvigy, D., Powers, J. S., Becknell, J. M., and Guan, K.: Diversity in plant hydraulic traits explains seasonal and inter-annual variations of vegetation dynamics in

- seasonally dry tropical forests, *New Phytol.*, 212, 80–95, <https://doi.org/10.1111/nph.14009>, 2016.
- Yu, L., Zeng, Y., Su, Z., Cai, H., and Zheng, Z.: The effect of different evapotranspiration methods on portraying soil water dynamics and ET partitioning in a semi-arid environment in Northwest China, *Hydrol. Earth Syst. Sci.*, 20, 975–990, <https://doi.org/10.5194/hess-20-975-2016>, 2016.
- Yu, L., Zeng, Y., Wen, J., and Su, Z.: Liquid-Vapor-Air Flow in the Frozen Soil, *J. Geophys. Res.-Atmos.*, 123, 7393–7415, <https://doi.org/10.1029/2018jd028502>, 2018.
- Zeng, Y. and Su, Z.: STEMMUS: Simultaneous Transfer of Energy, Mass and Momentum in Unsaturated Soil, University of Twente, Faculty of Geo-Information and Earth Observation (ITC), Enschede, 2013.
- Zeng, Y., Su, Z., Wan, L., and Wen, J.: A simulation analysis of the advective effect on evaporation using a two-phase heat and mass flow model, *Water Resour. Res.*, 47, W10529, <https://doi.org/10.1029/2011wr010701>, 2011a.
- Zeng, Y., Su, Z., Wan, L., and Wen, J.: Numerical analysis of air-water-heat flow in unsaturated soil: Is it necessary to consider airflow in land surface models?, *J. Geophys. Res.-Atmos.*, 116, D20107, <https://doi.org/10.1029/2011jd015835>, 2011b.
- Zhang, Y., Guanter, L., Joiner, J., Song, L., and Guan, K.: Spatially-explicit monitoring of crop photosynthetic capacity through space-based chlorophyll fluorescence data, *Remote Sens. Environ.*, 210, 362–374, <https://doi.org/10.1016/j.rse.2018.03.031>, 2018.
- Zhang, Z., Zhang, Y. G., Porcar-Castell, A., Joiner, J., Guanter, L., Yang, X., Migliavacca, M., Ju, W., Sun, Z., Chen, S., Martini, D., Zhang, Q., Li, Z., Cleverly, J., Wang, H., and Goulas, Y.: Reduction of structural impacts and distinction of photosynthetic pathways in a global estimation of GPP from space-borne solar-induced chlorophyll fluorescence, *Remote Sens. Environ.*, 240, 111722, <https://doi.org/10.1016/j.rse.2020.111722>, 2020.
- Zheng, Z. and Wang, G.: Modelling the dynamic root water uptake and its hydrological impact at the Reserva Jaru site in Amazonia, *J. Geophys. Res.-Biogeo.*, 112, G04012, <https://doi.org/10.1029/2007jg000413>, 2007.
- Zhou, S., Duursma, R. A., Medlyn, B. E., Kelly, J. W., and Prentice, I. C.: How should we model plant responses to drought? An analysis of stomatal and non-stomatal responses to water stress, *Agric. For. Meteorol.*, 182, 204–214, <https://doi.org/10.1016/j.agrformet.2013.05.009>, 2013.
- Zhou, S., Yu, B., Huang, Y., and Wang, G.: The effect of vapor pressure deficit on water use efficiency at the subdaily time scale, *Geophys. Res. Lett.*, 41, 5005–5013, <https://doi.org/10.1002/2014GL060741>, 2014.
- Zhou, S., Yu, B., Zhang, Y., Huang, Y., and Wang, G.: Partitioning evapotranspiration based on the concept of underlying water use efficiency, *Water Resour. Res.*, 52, 1160–1175, <https://doi.org/10.1002/2015wr017766>, 2016.
- Zhu, S., Chen, H., Zhang, X., Wei, N., Shangguan, W., Yuan, H., Zhang, S., Wang, L., Zhou, L., and Dai, Y.: Incorporating root hydraulic redistribution and compensatory water uptake in the Common Land Model: Effects on site level and global land modelling, *J. Geophys. Res.-Atmos.*, 122, 7308–7322, <https://doi.org/10.1002/2016jd025744>, 2017.
- Zhuang, J., Nakayama, K., Yu, G.-R., and Urushisaki, T.: Estimation of root water uptake of maize: an ecophysiological perspective, *Field Crop. Res.*, 69, 201–213, [https://doi.org/10.1016/s0378-4290\(00\)00142-8](https://doi.org/10.1016/s0378-4290(00)00142-8), 2001a.
- Zhuang, J., Yu, G., and Nakayama, K.: Scaling of root length density of maize in the field profile, *Plant Soil*, 235, 135–142, <https://doi.org/10.1023/A:1011972019617>, 2001b.